Appendix E – MIMO – Multiple Inputs – Multiple Outputs

In many ways, Multiple-Inputs – Multiple Output (MIMO) transmissions are obvious. A MIMO transmitter uses multiple antennas to transmit a data transmission, with a unique data transmission broadcast on each antenna. Each transmission is typically an identical wave form, and all the antennas broadcast on the same channel.

As each unique transmission propagates to the receiver, each experiences [different] multipath fading bases on its spatial relation to the environment. This fading alters the received signals relative to how they were synchronously broadcast, and alters each signal differently. Effectively, the receiver receives several signals on the same channel, but all all at different times. The receiver is configured with multiple antennas, too, so each signal is received on each configured antenna at sightly different times. With no real knowledge of the spatial relation of the transmitter (relative to the receiver), but with explicit knowledge of the antenna configuration of both the transmitter and receiver, the receiver can perform complex computations (basically solving a NxN matrix, where N is the number of antennas for the configuration) to reconstitute each unique signal from each antenna at the transmitter, thus reconstructing the original data streams.

In the past, multiple antennas on the same channel simply meant interference in the system. Today, however, with complex receivers, these data streams can maintain their integrity, not only in spite of multipath interference, but BECAUSE of the multipath fading. The multipath component is actually used to increase the individual signal-to-noise ratio for each signal, so long as significant multipath channels exist for a given configuration (frequency, topology, and antenna configuration).

MIMO can be combined with OFDM (Appendix D) to provide significant spectral efficiencies and data throughput gains.

References

[1] Alexander, Tom. Optimizing and Testing WLANs: Proven Techniques for Maximum Performance. Newnes, 2007.

[2] Patil, Basavaraj, et. al. IP in Wireless Networks. Upper Saddle River, NJ: Prentice Hall, 2003.

[3] "Official IEEE 802.11 Working Group Project Timelines – 2011-05-17." IEEE. <http://www.ieee802.org/11/Reports/802.11_Timelines.htm>, 2011.

[4] "Wi-Fi Alliance Is The New Name For WECA." Press Release. Wi-Fi Alliance. <http://www.wi-fi.org/news_articles.php?f=media_news&news_id=59>, 01 October 2002.

[5] Wi-Fi Alliance web site. <www.wi-fi.org>, 2011.

[6] Jabbusch, Jennifer (CISSP, HP MASE, JNCIA-AC), "A Brief History of Wireless Security." Security Uncorked. 18 August 2008. <http://securityuncorked.com/2008/08/history-of-wireless-security/>

[7] Jabbusch, Jennifer (CISSP, HP MASE, JNCIA-AC), "WEP Sucks, so Why are You Using It?" Security Uncorked. 18 August 2008. <http://securityuncorked.com/2008/08/history-of-wireless-security/>

[8] *IEEE Wireless LAN Medium Access Control (MAC) and Physical Layer (PHY) Specifications – Medium Access Control (MAC) Security Enhancements*, IEEE Amendment 802.11i-2004, 2004

[9] *IEEE Wireless LAN Medium Access Control (MAC) and Physical Layer (PHY) Specifications – Enhacements for Higher Throughput*, IEEE Amendment 802.11n-2009, 2009.

[10] *IEEE Wireless LAN Medium Access Control (MAC) and Physical Layer (PHY) Specifications*, IEEE Standard 802.11-2007, 2007.

[11] *IEEE Wireless LAN Medium Access Control (MAC) and Physical Layer (PHY) Specifications – Higher Speed Physical Layer Extension in the 2.4 GHz Band,* IEEE Amendment 802.11b-1999, 1999.

[12] "Channel Deployment Issues for 2.4-GHz 802.11 WLANs." Cisco Systems, Inc., <http://www.cisco.com/en/US/docs/wireless/technology/channel/deployment/guide/Channel.html>, 2004.

[13] *IEEE Wireless LAN Medium Access Control (MAC) and Physical Layer (PHY) Specifications – Further Higher Data Rate Extension in the 2.4 GHz Band*, IEEE Amendment 802.11g-2003, 2003.

[14] "Capacity Coverage & Deployment Considerations for IEEE 802.11g." Cisco Systems, Inc., <http://www.cisco.com/en/US/products/hw/wireless/ps4570/products_white_paper09186a00801d61a3.shtml>, 2005

[15] "Configure 802.11n on the WLC." Cisco Systems, Inc., <http://www.cisco.com/en/US/products/ps6366/products_tech_note09186a0080a3443f.shtml>, 2008.

[16] "Intel and 802.11." Intel Corporation, <http://www.intel.com/standards/case/case_8

02_11.htm>, 2011.

[17] *IEEE Wireless LAN Medium Access Control (MAC) and Physical Layer (PHY) Specifications – Specification for operation in additional regulatory domains*, IEEE Amendment 802.11d-2001, 2001.

[18] *IEEE Wireless LAN Medium Access Control (MAC) and Physical Layer (PHY) Specifications – Spectrum and Transmit Power Management Extensions in the 5 GHz band in Europe*, IEEE Amendment 802.11h-2003, 2003.

[19] *IEEE Wireless LAN Medium Access Control (MAC) and Physical Layer (PHY) Specifications – 4.9-5 GHz Operation in Japan*, IEEE Amendment 802.11j-2004. 2004.

[20] *IEEE Wireless LAN Medium Access Control (MAC) and Physical Layer (PHY) Specifications – Radio Resource Measurement of Wireless LANs*, IEEE Amendment 802.11k-2008, 2008.

[21] *IEEE Wireless LAN Medium Access Control (MAC) and Physical Layer (PHY) Specifications – Wireless Access in Vehicular Environments*, IEEE Amendment 802.11p-2010, 2010.

[22] *IEEE Wireless LAN Medium Access Control (MAC) and Physical Layer (PHY) Specifications – Fast Basic Service Set (BSS) Transition*, IEEE Amendment 802.11r-2008, 2008.

[23] *IEEE Wireless LAN Medium Access Control (MAC) and Physical Layer (PHY) Specifications – Internetworking with External Networks*, IEEE Amendment 802.11u-2011, 2011.

[24] *IEEE Wireless LAN Medium Access Control (MAC) and Physical Layer (PHY) Specifications – IEEE 802.11 Wireless Network Management*, IEEE Amendment 802.11v-2011, 2011.

[25] *IEEE Wireless LAN Medium Access Control (MAC) and Physical Layer (PHY) Specifications – Protected Management Frames*, IEEE Amendment 802.11w-2009, 2009.

[26] *IEEE Wireless LAN Medium Access Control (MAC) and Physical Layer (PHY) Specifications – 3650-3700 MHz Operation in USA*, IEEE Amendment 802.11y-2008, 2008.

[27] *IEEE Wireless LAN Medium Access Control (MAC) and Physical Layer (PHY) Specifications – Extensions to Direct-Link Setup (DLS)*, IEEE Amendment 802.11z-201, 2010.

[28] Schneier, Bruce. Beyond Fear: Thinking Sensibly About Security in an Uncertain World. Springer, 2003.

[29] Security Rules and Procedures-Merchant Edition, Mastercard Worldwide, <http://www.mastercard.com/global/merchant/_assets/docs/SecurityRules&Procedures.pdf>, 29 January 2010.

[30] Schneier, Bruce. "My Open Wireless Network." Schneier on Security, <http://www.schneier.com/blog/archives/2008/01/my_open_wireles.html>, 2008

[31] Fourozan, Behrouz A., Data Communications and Networking, New York, NY: McGraw-Hill, 2004.

[32] *Federal Standard 1037C – Telecommunications: Glossary of Telecommunications Terms*, Institute for Telecommunications Sciences, 07 August, 1996.

[33] Weigle, Dr. Michele. "WAVE/DSRC/802.11p." Old Dominion University, Spring 2008.

[34] AODV, University of California, Santa Barbara, <http://moment.cs.ucsb.edu/AODV/>, 2004.

[35] Camp, Joseph D. and Knightly, Edward W. "The IEEE 802.11s Extended Service Sett Mesh Networking Standard", IEEE Communications Magazine, August 2008

[36] Wexler, Joanie. "Latest Wi-Fi standard amendment could aid in Wi-Fi offload," Network World, Feruary 25, 2011.

[37] Van Nee, Richard, Qualcomm Inc., "Breaking the Gigabit-Per-Second Barrier with 802.11ac." IEEE Wireless Communications, April 2011.

[38] Vaughan-Nichols, Steven J., "Gigabit Wi-Fi Is on Its Way." Computer (IEEE Journal), November 2010.

[39] Sum, Chin-Sean, et al. "Smart utility networks in tv white space." IEEE Communications Magazine, 30 June 2011.

[40] Shin, Kang G. et al. "Cognitive Radios for Dynamic Spectrum Access: From Concept to Reality," IEEE Wireless Communications, December 2010.

Appendix XXVII. Thinh Pham, et al., *Shaping Spectral Leakage for IEEE 802.11p Vehicular Communications*, VEHICULAR TECHNOLOGY CONFERENCE (VTC SPRING), May 2014.

Shaping Spectral Leakage for IEEE 802.11p Vehicular Communications

Thinh H. Pham*, Ian Vince McLoughlin†, Suhaib A. Fahmy*
*School of Computer Engineering
Nanyang Technological University, Singapore
Email: hung3@e.ntu.edu.sg
†School of Information Science and Technology
University of Science and Technology of China, Hefei, China

***Abstract*—IEEE 802.11p is a recently defined standard for the physical (PHY) and medium access control (MAC) layers for Dedicated Short-Range Communications. Four Spectrum Emission Masks (SEMs) are specified in 802.11p that are much more stringent than those for current 802.11 systems. In addition, the guard interval in 802.11p has been lengthened by reducing the bandwidth to support vehicular communication (VC) channels, and this results in a narrowing of the frequency guard. This raises a significant challenge for filtering the spectrum of 802.11p signals to meet the specifications of the SEMs. We investigate state of the art pulse shaping and filtering techniques for 802.11p, before proposing a new method of shaping the 802.11p spectral leakage to meet the most stringent, class D, SEM specification. The proposed method, performed at baseband to relax the strict constraints of the radio frequency (RF) front-end, allows 802.11p systems to be implemented using commercial off-the-shelf (COTS) 802.11a RF hardware, resulting in reduced total system cost.**

I. Introduction

Dedicated Short-Range Communications (DSRC) refers to the provision of a wireless channel for new vehicular safety applications through vehicle-to-vehicle (V2V) and Road to Vehicle (RTV) communications. In 2010 the IEEE defined a standard for DSRC's PHY and MAC layers [1], named IEEE 802.11p. The PHY in 802.11p is largely inherited from the well-established IEEE 802.11a OFDM PHY, with several changes aimed at improving performance in vehicular environments. The advantage of building on 802.11a is a significant reduction in the cost and development effort necessary to develop 802.11p hardware and software. It also plays an important role in allowing backwards compatibility from 802.11p to 802.11a [2], [3].

Essentially, three changes are made in IEEE 802.11p [4]: First, 802.11p defines a 10 MHz channel width instead of the 20 MHz used by 802.11a. This extends the guard interval to address the effects of Doppler spread and inter-symbol interference in a VC channel. Secondly, 802.11p defines several improvements in receiver adjacent channel rejection performance to reduce the effect of cross channel interference that is especially important in vehicle communication channels. Finally, 802.11p defines four spectral emission masks (SEMs) corresponding to class A to D operations that are specified and issued in FCC CFR47 Sections 90.377 and 95.1509. These are more stringent than for current 802.11 radios, in order to improve performance in urban vehicle scenarios.

Thanks to the similarities between the two PHYs, some work has focused on making 802.11a PHY devices compatible with 802.11p [5], [6], [2]. Most researchers deal with the transformation in four parts, namely, reducing channel bandwidth, channel estimation, transmission power requirements, and effective channel access performance. Due to a dearth of affordable 802.11p prototype hardware, existing wireless testbeds for 802.11p tend to use modified commercial off-the-shelf (COTS) 802.11a hardware [5]. For example, Almeda and Matos present a front-end using 802.11a hardware that is targeted to comply with the specification of 802.11p [7]. Despite strict constraints, it still does not meet the SEM requirement. Fuxjäger et al. present an implementation of a fully functional 802.11p transmitter using GNU Radio, a software-defined radio platform [8]. However, the output signal spectrum contains two peaks caused by image frequencies, which the output filter is unable to remove. Hence, it does not even satisfy class A. Contrast this to an early prototype transceiver, based on a modified Atheros chip set [8], which fulfils class A requirements, but can not meet class C specifications. The consequence of the stringent SEMs significantly increases the difficulty, and hence cost, of implementing new silicon or hardware for 802.11p. To the best of the authors' knowledge, there are no published implementations or testbeds for 802.11p that are able to meet the class D specifications. There remains a debate regarding whether and when chip makers will be able to meet such requirements [4].

To relax the stringent specification of the SEMs, additional signal processing at baseband is investigated in this paper for spectral leakage filtering of the 802.11p OFDM signal. Increasing processing at baseband to address this challenge is a sensible approach as much of the baseband processing is done on optimised processors or FPGAs [17], where the relative increase in computational cost can be easily tolerated. In particular, this paper contributes a new method for filtering the OFDM signal at baseband in an effort to fulfil the stringent class D specifications of the IEEE 802.11p standard.

II. Signal Model

We consider an 802.11p OFDM symbol to have inverse fast Fourier transform (IFFT) length and cyclic prefix (CP) length of $N = 64$ and $N_{CP} = 16$, respectively. Therefore, the length of an 802.11p symbol including CP is $N_T = N + N_{CP} = 80$. A sample $x(m)$ of the OFDM symbol $(0 \leq m \leq N_T - 1)$ in the time domain can be expressed as

$$x(m) = \frac{1}{N} \sum_{k=0}^{N-1} X(k) e^{i2\pi \frac{k}{N}(m - N_{CP})}, \quad (1)$$

where $X(k)$ is the frequency domain representation of data subcarriers. Typically, the OFDM symbol samples are transmitted sequentially, which is equivalent to multiplying symbols with a rectangular window function, p. The transmitted samples of 802.11p signal can be expressed as;

$$x(n) = \frac{1}{N} \sum_{l=-\infty}^{\infty} \sum_{k=0}^{N-1} X(k) p(n - lN_T) e^{i2\pi \frac{k}{N}(n - N_{CP} - lN_T)} \quad (2)$$

The 802.11p symbol has 16 samples for CP (i.e. the same as in 802.11a). The CP is a guard interval inserted to avoid inter-symbol interference (ISI) when OFDM symbols are transmitted over a delay-dispersive multi-path channel, represented by a channel impulse response (CIR) with length h, derived from the delay spread of the channel. If the CP is shorter than the channel delay, ISI will be present in received symbols. Unfortunately, the 802.11p VC channel tends to experience a larger delay spread than WLAN: according to empirical VC channel models in [9], [10], maximum delay spread varies depending on different propagation models and traffic environment. The RTV model for suburban street, urban canyon, and expressway, have maximum excess delay of 700, 501, and 401 ns, respectively [9]. For the V2V model, measurements in [10] show that delay spread is largest for urban areas and smallest for highway areas. The 90% measured value of delay spread for urban areas is near 600 ns. In 802.11p, guard intervals are lengthened to avoid ISI, but this raises some challenges in the frequency domain. First, reducing bandwidth requires a higher quality factor front-end filter circuit for the higher frequency carrier compared to 802.11a. Second, in an 802.11p system, similar to 802.11a, there are 6 subcarrier spacings used for the frequency guard per side. But reducing the sampling frequency leads to a narrowing of the frequency guard. Generally, to improve performance in VC channels with large delay spread, the timing guard is increased, narrowing the frequency guard and resulting in more strict filtering constraints.

In addition, 802.11p will operate in the 5.9 GHz DSRC spectrum divided into seven 10 MHz bands. This channelization allows the MAC upper layer, i.e., IEEE 1609.4, to perform multi-channel operations [11]. The mechanism allows safety and other applications to occupy separate channels to reduce interference. The four 802.11p SEMs are defined to reduce the effect of ICI. Wu et al. [12] showed that transmitters on adjacent service channels still cause inter-channel interference (ICI) in the safety channel, even if they satisfy the class C requirement. Shaping 802.11p spectral leakage is thus potentially important in helping to eliminate ICI.

III. Using Pulse Shaping for 802.11p

Pulse shaping (using a smooth rather than rectangular pulse), recommended in 802.11a, is effective at reducing side lobes, though it can induce distortion in the subcarriers. One way to avoid this is to add extending parts, i.e. CP and a cyclic suffix (CS) before and after each conventional OFDM symbol respectively, and to multiply the extended symbol with a smoothing function. While the CP in conventional OFDM is used as a guard interval, here it is also used for pulse shaping.

Pulse shaping extends the N_T length of the OFDM signal by a roll-off factor, β. The overhead of extending CS results in spectral loss; overlapping of the CP and CS of consecutive symbols shown in Fig. 1 is needed to form a transmitted symbol to reduce this loss, but causes ISI in the overlapped region.

Pulse shaping using the overlapping method is effectively equivalent to shortening the OFDM guard interval. A larger β obtains greater compression in spectral leakage but reduces the effective guard interval. When βN_T is increased to equal the CP length, the effective guard interval is reduced to zero (no guard interval) to prevent channel-induced ISI. Three state-of-the-art smoothing functions for pulse shaping are investigated. The first is present in the IEEE 802.11a standard. The second is based on a raised cosine function proposed by Bala et al. [13]. The last is based on the characteristics of functions with vestigial symmetry presented by Castanheira and Gameiro [14]. The three functions are rewritten in discrete form in Equations (3), (4), (5), respectively.

$$p_1 = \begin{cases} sin^2(\frac{\pi}{2}(0.5 + \frac{m}{2\beta N_T})), & 0 \leq m < \beta N_T \\ 1, & \beta N_T \leq m < N_T \\ sin^2(\frac{\pi}{2}(0.5 - \frac{m - N_T}{2\beta N_T})), & N_T \leq m < (1+\beta)N_T \end{cases} \quad (3)$$

$$p_2 = \begin{cases} \frac{1}{2} + \frac{1}{2}cos(\pi(1 + \frac{m}{\beta N_T})), & 0 \leq m < \beta N_T \\ 1, & \beta N_T \leq m < N_T \\ \frac{1}{2} + \frac{1}{2}cos(\pi(1 + \frac{m - N_T}{\beta N_T})), & N_T \leq m < (1+\beta)N_T \end{cases} \quad (4)$$

$$p_3 = \begin{cases} \frac{1}{2} + \frac{9}{16}cos(\pi(1 - \frac{m}{\beta N_T})) \\ -\frac{1}{16}cos(3\pi(1 - \frac{m}{\beta N_T})), & 0 \leq m < \beta N_T \\ 1, & \beta N_T \leq m < N_T \\ \frac{1}{2} + \frac{9}{16}cos(\pi\frac{m - N_T}{\beta N_T}) \\ -\frac{1}{16}cos(3\pi\frac{m - N_T}{\beta N_T}), & N_T \leq m < (1+\beta)N_T \end{cases} \quad (5)$$

The decay of OFDM spectral side lobes using pulse shaping is first investigated by assuming that the effect of image spectrum caused by interpolation or digital-to-analog conversion (DAC) is negligible. This assumption is made because the band gap between 802.11p spectrum and its image spectrum is relatively narrow. The image spectrum can affect the ability to shape spectrum leakage (this is investigated later). Fig. 2 shows simulation results for three smoothing functions with respect to the image spectrum.

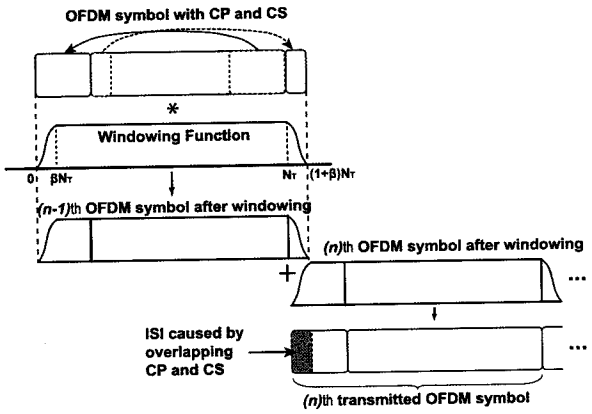

Fig. 1. Pulse Shaping operation performed on OFDM symbols.

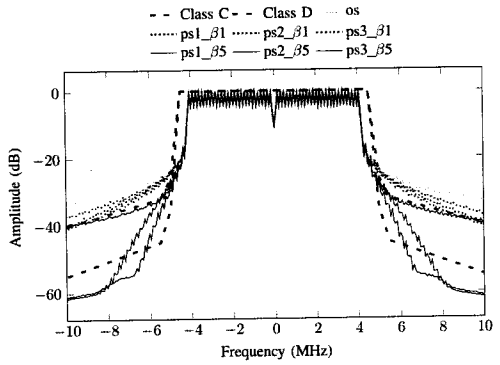

Fig. 2. Spectrum of pulse shaping OFDM symbols using three smoothing functions.

os is the original OFDM spectrum without using pulse shaping. $ps1\_\beta1$, $ps2\_\beta1$, $ps3\_\beta1$ denote the spectrum of the OFDM signal using smoothing functions: $p_1(m)$, $p_2(m)$, $p_3(m)$, respectively with roll-off factors chosen as $\beta N_T = 1$ Similarly, $ps1\_\beta5$, $ps2\_\beta5$, $ps3\_\beta5$ present the spectrum of OFDM signals with $\beta N_T = 5$. In the case of using one guard interval sample, the spectral leakage is reduced compared to the original OFDM signal. $p_1(m)$ obtains better results in comparison to the other two, however, the shaped spectra still do not meet the requirement of class C. When 5 samples of CP are used for pulse shaping, shaping spectrum leakage using $p_2(m)$ and $p_3(m)$ achieves a significant improvement. The spectrum using $p_2(m)$ satisfies class C and almost meets the requirement of class D. Ignoring the presence of an image spectrum, the pulse shaping method can take part of the guard interval for applying the smoothing function in order to shape the spectral leakage and achieve stringent SEM compliance. Fig. 3 shows simulation results for pulse shaping 802.11p OFDM symbols with the presence of the image spectrum.

The spectrum of OFDM signals using pulse shaping in Fig. 3 is almost identical to (but slightly better than) the original OFDM signal. With the presence of an image spectrum, pulse shaping does not obtain significant improvement in terms of limiting the spectrum leakage in 802.11p. The band gap between the main spectrum and the image spectrum is not

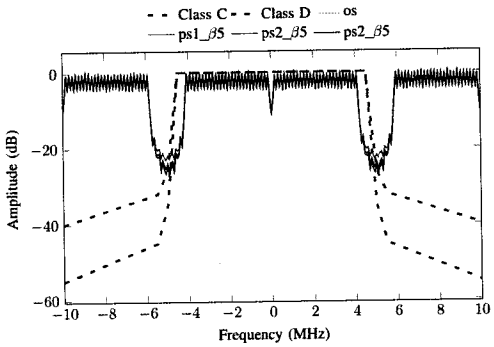

Fig. 3. Spectrum of pulse shaping 802.11p OFDM symbols with the presence of the image spectrum.

large enough for pulse shaping to obtain a significant spectral leakage decay. Hence, this method does not help to cancel the image spectrum caused by interpolation or DAC. The next section investigates applying an FIR filter to cancel the image spectrum.

IV. Image Spectrum Cancellation By FIR Filter

The critical issue for 802.11p signals meeting the stringent requirements of the class D mask is that the frequency guards are narrow and the frequency carrier is relatively high (5.9 GHz) compared to 802.11a. Interpolation can be used at baseband to increase sampling frequency, thereby extending baseband bandwidth. Image spectra are repeats of the original baseband spectrum, present because of interpolation effects. An interpolation filter, commonly implemented as an FIR filter, may be used to cancel image spectra.

On one hand, the narrow band gap between main and adjacent image spectra requires a long impulse response FIR filter. On the other hand, the impulse response of the FIR filter has a similar effect to the impulse response of the overall channel in terms of inducing ISI. The FIR filter reduces the effective guard interval of OFDM symbols [15]. Its design also needs to deal with the tradeoff between the length of filter to avoid ISI and the transition band and attenuation of the filter to meet the requirement of SEMs. We investigate several widely used FIR filters, listed in Table I, as applied to 802.11p. An empirical formula [16] is used to estimate the length of each filter in terms of attenuation A and transition band $\Delta\omega$. The specifications of the class D SEM for 802.11p are used to calculate the required number of taps with L-fold interpolation. The required lengths of these FIR filters for 802.11p are larger than the guard interval of the 802.11p symbol.

To avoid ISI, the maximum length of the FIR filter is derived by taking into account guard interval and CIR. By assuming that the delay spread of the VC channel is constrained to a maximum of 600 ns (see Section 2), CIR is equivalent to 6 samples of the 802.11p guard interval. That assumption is based on the result of the channel model in [9], [10]. Therefore, the effective guard interval remains 10 samples for filtering. In addition, when the filter is used in a transmitter, a matched filter is required at the receiver [15] resulting in 5 samples of guard interval for transmitter filtering. L-fold

TABLE I
POPULAR WINDOW-BASED FIR FILTER LENGTHS

Window	Stopband Atten.	Filter Len.	Length for 802.11p
Hamming	-26.5dB	$N = \frac{6.22\pi}{\Delta\omega}$	$N \approx 31L$
Hanning	-31.5dB	$N = \frac{6.65\pi}{\Delta\omega}$	$N \approx 33L$
Backman	-42.7dB	$N = \frac{11.1\pi}{\Delta\omega}$	$N \approx 55L$
Kaiser	—	$N = \frac{A-7.95}{2.23\Delta\omega}, A > 21$ $N = \frac{5.79}{\Delta\omega}, A < 21$	$N \approx 33L$
Chebyshev	—	$N = \frac{2.06A-16.5}{2.29\Delta\omega}$	$N \approx 67L$

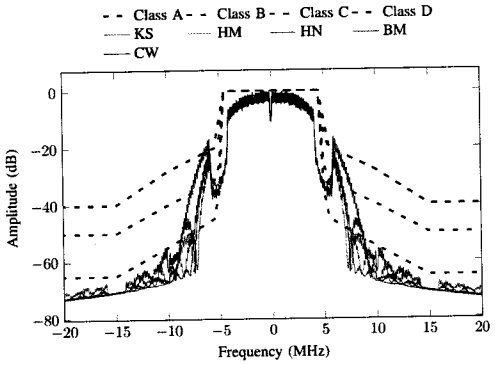

Fig. 4. Spectra of filtered OFDM symbols for 802.11p using different FIR filters.

interpolation is used at the transmitter. Therefore, the permitted length of the FIR filters is $5 \times L$, and that is applied to design the FIR filters. A simulation is performed with $L = 8$ to evaluate filtered spectra for the 802.11p signal. These FIR filters are employed to filter the interpolated OFDM signal, and the results of the filtered spectra are presented in Fig. 4.

KS, HM, HN, BM, CW denote the filtered spectra obtained by using Kaiser, Hamming, Hanning, Blackman, Chebyshev windows, respectively. Applying the filters causes two wide auxiliary peaks beside the main spectrum. The Blackman window filtered spectrum slightly exceeds the requirement of class A. That of the remaining window filters does meet the requirements of classes A and B but not of classes C and D. Hence, given the effective guard interval of 802.11p, FIR filtering does not provide a solution.

V. PROPOSED METHOD

This section proposes a novel method for achieving the class D specification. The proposed method relies upon spectrum manipulation, using the extending frequency guard technique, allied with pulse shaping and an FIR filter. It is performed in a specified procedure with the following steps: first, the frequency guard is extended [15] by increasing the size of the IFFT to M times the original IFFT. The sampling frequency is also increased M times to maintain the same subcarrier spacing. The data symbols employ lower sub-carriers that are the same as those in the original IFFT. The remaining sub-carriers are zero-padded, resulting in extending the frequency guard. Second, pulse shaping is employed to shape the spectral

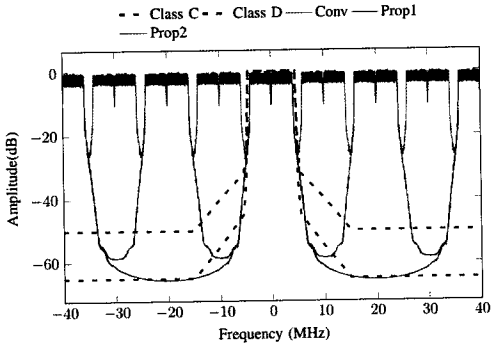

Fig. 5. Spectrum of 802.11p signal of the proposed method after interpolation.

leakage to meet the specification of class D. Third, L-fold interpolation is performed to extend the baseband spectrum and hence relax the requirement of the RF front-end hardware. Finally, thanks to the extended frequency guard, a short length FIR filter can easy filter out the final image spectrum caused by interpolation.

Continuing the assumption from Section IV, the CIR length does not exceed 600 ns. Therefore, the effective guard interval which is equivalent to the length of 10 samples of the original CP, i.e., $10 \times 100 = 1000\ ns$ is used for the pulse shaping and FIR filter. By choosing an DAC sampling frequency of 80 MHz, the sampling frequency of 802.11p is increased by 8 times compared to the original (10 MHz). Two options denoted as $Prop1$, $Prop2$ are studied. $Prop1$ doubles the size of IFFT, i.e., $M = 2$, this means doubling the sampling frequency, to extend the frequency guard. Then 4-fold interpolation, i.e., $L = 4$, is required to obtain a sampling frequency of 80 MHz. $Prop2$ quadruples the size of IFFT, i.e., $M = 4$; Then 2-fold interpolation, i.e., $L = 2$, is performed to maintain the sampling frequency at 80 MHz. Based on the results in section III, $p_2(m)$ is employed with $\beta N_T = 5 \times M$, that is equivalent to the length of 5 samples of the original CP, i.e., 500 ns. It should be noted that after extending the frequency guard, the number of samples in the symbol including CP, is increased M times. Fig. 5 shows the shaped spectrum of the proposed method after interpolation in the baseband, at 80 MHz. The result is also compared to the original spectrum denoted *Conv*, and the specifications of classes C and D. The main spectrum of $Prop1$, $Prop2$ almost satisfy class D. The image spectrum of $Prop1$ is present at ± 40 MHz and ± 20 MHz whilst $Prop2$ has an image spectrum at ± 40 MHz.

A simple short length FIR filter is needed to cancel the image spectra. The remaining guard interval for the transmitter filter and matched filter is 500 ns. Therefore, the maximum impulse response of the FIR filter is 250 ns, which is equivalent to $2.5 \times M \times L$ samples at the 80 MHz sampling frequency.

FIR filters are designed for $Prop1$, $Prop2$ using a Kaiser window. Because the frequency guard of $Prop1$ is still relatively narrow, it requires an FIR filter with the length of 20 samples to cancel the image spectrum. Fig. 6 shows the result of spectrum filtering for $Prop1$ in comparison to the original

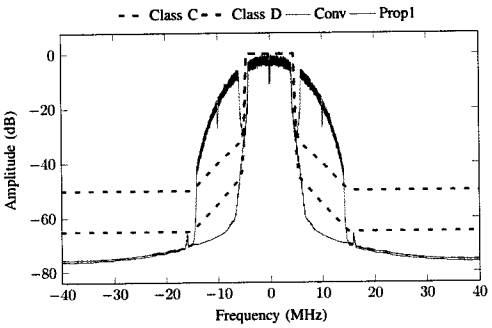

Fig. 6. Filtered Spectrum of 802.11p signal using option *Prop*1.

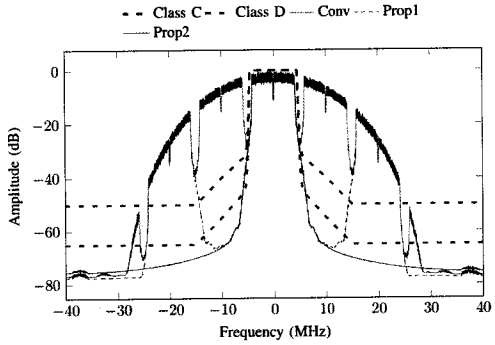

Fig. 7. Filtered Spectrum of 802.11p signal using option *Prop*2.

OFDM spectrum and class C, D SEMs. As can be seen in the *Prop*1 spectrum, there are still two small peaks caused by the image spectrum. These peaks are compressed by the FIR filter to meet the class D requirement. Slight distortion is present in the main spectrum because of the effect of the FIR filter. *Prop*2 has a wider frequency guard compared to *Prop*1. The FIR filter only requires a length of 12 samples to cancel the image spectrum and the remaining effective guard interval of 200 ns is reserved. Fig. 7 shows the result of spectral filtering for *Prop*2 and *Prop*1 with respect to the class C and D SEMs. The image spectrum of *Prop*2 can be cancelled by a short length FIR filter whilst the image spectrum of *Prop*1 still remains larger in magnitude. Hence, *Prop*2 meets the class D specification.

The simulation results demonstrate that the proposed technique for shaping spectral leakage can meet the specification of class D, the most stringent of the four 802.11p SEMs. *Prop*2 obtains better performance in terms of distortion and effective guard interval compared to *Prop*1, but pays the cost of a higher computational requirement due to the increased IFFT size. It should be noted that the additional computation needed for signal processing in the baseband (which contains low cost, power components), can be repaid by relaxing the specification of the RF front-end design (which tends to require more costly, and higher power components).

VI. Conclusion

This paper has investigated the shaping of leakage spectrum for 802.11p at the baseband. The narrow frequency guard defined in 802.11p does not allow common pulse shaping techniques to perform well, ruling out many methods developed for 802.11a. The 802.11p guard interval is not long enough for an FIR filter to perfectly cancel the image spectrum caused by interpolation or the DAC process. A new leakage spectrum shaping method was proposed for 802.11p systems. It entails performing filtering based upon the extending the frequency guard, allied with careful pulse shaping, and simple (much shorter) FIR filtering. Simulations show that the proposed method can meet the specification of class D, the most stringent of the four 802.11p SEMs.

References

[1] *IEEE 802 Standard; Part 11; Amendment 6: Wireless Access in Vehicular Environments*, IEEE std. 802.11p, Jul. 2010.

[2] W. Vandenberghe, I. Moerman, and P. Demeester, "Approximation of the IEEE 802.11p standard using commercial off-the-shelf IEEE 802.11a hardware," in *International Conference on ITS Telecommunications (ITST)*, 2011, pp. 21–26.

[3] J. Fernandez, K. Borries, L. Cheng, B. Kumar, D. Stancil, and F. Bai, "Performance of the 802.11p Physical Layer in Vehicle-to-Vehicle Environments," *IEEE Transactions on Vehicular Technology*, vol. 61, no. 1, pp. 3–14, 2012.

[4] D. Jiang and L. Delgrossi, "IEEE 802.11p: Towards an International Standard for Wireless Access in Vehicular Environments," in *IEEE Vehicular Technology Conference (VTC)*, 2008, pp. 2036–2040.

[5] D. Lo Iacono and T. Cupaiuolo, "Power Efficient SDR Implementation of IEEE 802.11a/p Physical Layer," *Journal of Signal Processing Systems*, vol. 73, no. 3, pp. 281–289, 2013.

[6] W.-Y. Lin, M.-W. Li, K.-C. Lan, and C.-H. Hsu, "A Comparison of 802.11a and 802.11p for V-to-I Communication: A Measurement Study," in *Quality, Reliability, Security and Robustness in Heterogeneous Networks*. Springer, 2012, vol. 74, pp. 559–570.

[7] N. de Almeida, J. Matos, and J. Lopes, "A front end to vehicular communications," in *IEEE International Conference on Computer as a Tool (EUROCON)*, 2011, pp. 1–4.

[8] P. Fuxjäger, A. Costantini, D. Valerio, P. Castiglione, G. Zacheo, T. Zemen, and F. Ricciato, "IEEE 802.11 p transmission using GNURadio," in *Proceedings of the Karlsruhe Workshop on Software Radios (WSR)*, 2010, pp. 83–86.

[9] G. Acosta-Marum and M.-A. Ingram, "Six time and frequency selective empirical channel models for vehicular wireless LANs," *IEEE Vehicular Technology Magazine*, vol. 2, no. 4, pp. 4–11, 2007.

[10] I. Sen and D. Matolak, "Vehicle - Vehicle Channel Models for the 5-GHz Band," *IEEE Transactions on Intelligent Transportation Systems,*, vol. 9, no. 2, pp. 235–245, 2008.

[11] *IEEE Standard for Wireless Access in Vehicular Environments-Multi-Channel Operations*, IEEE Std 1609.4-2010, Dec. 2010.

[12] X. Wu, S. Subramanian, R. Guha, R. White, J. Li, K. Lu, A. Bucceri, and T. Zhang, "Vehicular Communications Using DSRC: Challenges, Enhancements, and Evolution," *IEEE Journal on Selected Areas in Communications*, vol. 31, no. 9, pp. 399–408, 2013.

[13] E. Bala, J. Li, and R. Yang, "Shaping Spectral Leakage: A Novel Low-Complexity Transceiver Architecture for Cognitive Radio," *IEEE Vehicular Technology Magazine*, vol. 8, no. 3, pp. 38–46, 2013.

[14] D. Castanheira and A. Gameiro, "Novel Windowing Scheme for Cognitive OFDM Systems," *IEEE Wireless Communications Letters*, vol. 2, no. 3, pp. 251–254, 2013.

[15] B. Farhang-Boroujeny, *Signal processing techniques for software radios*. Lulu publishing house, 2008.

[16] R. J. Kapadia, *Digital Filters Theory, Application and Design of Modern Filters*. Wiley-VCH, 2012.

[17] J. Lotze, S. A. Fahmy, J. Noguera, B. Ozgül, L. Doyle, and R. Esser, "Development framework for implementing FPGA-based cognitive network nodes," in *Proceedings of the IEEE Global Communications Conference (GLOBECOM)*, 2009.

Appendix XXVIII. NHTSA, *Vehicle Safety Communications– Applications Final Report: Appendix 2 Communications and Positioning* (Sept. 2011).

U.S. Department
of Transportation
**National Highway
Traffic Safety
Administration**

NHTSA
www.nhtsa.gov

DOT HS 811 492C

September 2011

Vehicle Safety Communications – Applications (VSC-A)

Final Report: Appendix Volume 2 Communications and Positioning

CAMP

Vehicle Safety Communications 2

Mercedes-Benz Research & Development North America, Inc.

GM

TOYOTA

HONDA

Honda R&D Americas, Inc.

Ford

Intelligent Transportation Systems

DISCLAIMER

This publication is distributed by the U.S. Department of Transportation, National Highway Traffic Safety Administration, in the interest of information exchange. The opinions, findings, and conclusions expressed in this publication are those of the authors and not necessarily those of the Department of Transportation or the National Highway Traffic Safety Administration. The United States Government assumes no liability for its contents or use thereof. If trade names, manufacturers' names, or specific products are mentioned, it is because they are considered essential to the object of the publication and should not be construed as an endorsement. The United States Government does not endorse products or manufacturers.

Technical Report Documentation Page

1. Report No.	2. Government Accession No.	3. Recipient's Catalog No.
DOT HS 811 492C		

4. Title and Subtitle	5. Report Date
Vehicle Safety Communications – Applications (VSC-A) Final Report: Appendix Volume 2 Communications and Positioning	September 2011
	6. Performing Organization Code

7. Authors	8. Performing Organization Report No.
Ahmed-Zaid, F., Bai, F., Bai, S., Basnayake, C., Bellur, B., Brovold, S., Brown, G., Caminiti, L., Cunningham, D., Elzein, H., Hong, K., Ivan, J., Jiang, D., Kenney, J., Krishnan, H., Lovell, J., Maile, M., Masselink, D., McGlohon, E., Mudalige, P., Popovic, Z., Rai, V., Stinnett, J., Tellis, L., Tirey, K., VanSickle, S.	

9. Performing Organization Name and Address	10. Work Unit No. (TRAIS)
Crash Avoidance Metrics Partnership on behalf of the Vehicle Safety Communications 2 Consortium 27220 Haggerty Road, Suite D-1 Farmington Hills, MI 48331	11. Contract or Grant No. DTNH22-05-H-01277

12. Sponsoring Agency Name and Address	13. Type of Report and Period Covered
NHTSA Headquarters 1200 New Jersey Avenue, SE West Building Washington, DC 20590 **Research and Innovative Technology Administration** U.S. Department of Transportation 1200 New Jersey Avenue, SE East Building Washington, DC 20590	Final Report Dec. 8, 2006, through Dec. 7, 2009 14. Sponsoring Agency Code

15. Supplementary Notes

16. Abstract

The Vehicle Safety Communications – Applications (VSC-A) Project was a three-year project (December 2006 - December 2009) to develop and test communications-based vehicle-to-vehicle (V2V) safety systems to determine if Dedicated Short Range Communications (DSRC) at 5.9 GHz, in combination with vehicle positioning, can improve upon autonomous vehicle-based safety systems and/or enable new communications-based safety applications. The VSC-A Project was conducted by the Vehicle Safety Communications 2 Consortium (VSC2). Members of VSC2 are Ford Motor Company, General Motors Corporation, Honda R & D Americas, Inc., Mercedes-Benz Research and Development North America, Inc., and Toyota Motor Engineering & Manufacturing North America, Inc. This document presents the second volume set of appendices for the Final Report of the VSC-A Project which contains technical content for the Communications Power Testing, Multi-Channel Operations, Relative Positioning Software Performance Analysis, GPS Service Availability Study Literature Review and Final Report, and Multiple-OBE Scalability Testing Results.

17. Key Word	18. Distribution Statement
	Document is available to the public from the National Technical Information Service www.ntis.gov

19. Security Classif. (of this report)	20. Security Classif. (of this page)	21. No. of Pages	22. Price
Unclassified	Unclassified	339	

Form DOT F 1700.7 (8-72) Reproduction of completed page authorize

Table of Contents

VSC-A Final Report: Appendix D-1

Communications Power Testing

List of Acronyms

BSW	Blind Spot Warning
CAMP	Crash Avoidance Metrics Partnership
CLW	Control Loss Warning
dBm	Decibels relative to 1 Milliwatt
DGPS	Differential GPS
DNPW	Do Not Pass Warning
DSRC	Dedicated Short Range Communications
EEBL	Emergency Electronic Brake Lights
EIRP	Equivalent Isotropically Radiated Power
EVM	Error Vector Magnitude
FCW	Forward Collision Warning
GPS	Global Positioning System
IMA	Intersection Movement Assist
ITS	Intelligent Transportation Systems
LCW	Lane Change Warning
LOS	Line Of Sight
Mbps	MegaBits Per Second (10^6 bits/second)
NHTSA	National Highway Traffic Safety Administration
NLOS	Non Line Of Sight
PER	Packet Error Rate
RF	Radio Frequency
RSSI	Received Signal Strength Indication
VSC2	Vehicle Safety Communications 2
VSC-A	Vehicle Safety Communications – Applications
V-V or V2V	Vehicle-to-Vehicle
WSU	Wireless Safety Unit

Table of Contents

List of Figures

List of Tables

1 Overview

The purpose of the VSC-A Power Testing activity is to measure the relationship between transmission power and packet reception performance in the Dedicated Short Range Communication (DSRC) band. Sending messages with greater power has the potential to improve message reception at far ranges or around obstructions. However, increasing transmission power has potential problems as well. Higher transmission power generally leads to a larger interference range and, thereby, increases channel loading and congestion. High power transmissions are also subject to a tighter spectral mask.

Transmission characteristics with reduced power are also of interest. As the transmission range decreases, the scope of the shared wireless "channel" shrinks, which can be an effective tool in alleviating packet congestion. This advantage must be balanced, however, against any reduced effectiveness of safety applications that results from the smaller transmission range.

These tests provided the VSC-A team with a robust understanding of how transmission power, fading, and obstacles affect message reception. Various propagation environments were considered: urban, suburban, rural, and highway.

The principal work item of this activity is to fully characterize packet reception probability as a function of transmission power, occlusions (e.g., trucks, buildings, etc.), distance, multi-path environment, and bit rate.

This report documents the test setup, test scenarios, and associated power testing results.

2 Testing Overview

The test cases for are designed to address two specific issues:

1. Identify environments in which the improved reception performance associated with higher transmission powers may be useful for the VSC-A applications
2. Improve our understanding of the limitations of communication performance for both high power and lower power communications

For these tests 20 dBm is defined as the "nominal" transmission power for DSRC messages. Transmission levels above 20 dBm are defined as "high" power, and transmission levels below 20 dBm are defined as "low" power.

2.1 Relevant VSC-A Applications

The VSC-A Project has defined 6 safety applications to be developed.

1. Emergency Electronic Brake Lights (EEBL)
2. Forward Collision Warning (FCW)
3. Do No Pass Warning (DNPW)
4. Control Loss Warning (CLW)
5. Intersection Movement Assist (IMA)

6. Blind Spot Warning+Lane Change Warning (BSW+LCW)

From a power testing perspective, a number of these applications are primarily concerned with traffic traveling along a single axis. It follows that the test scenarios motivated by these applications individually are largely overlapping. This point is reinforced by the observation that a single lane of lateral offset between two vehicles will not produce a notably different power test result than a same-lane alignment. Thus, if an application is concerned with AHEAD-LEFT, AHEAD, and AHEAD-RIGHT alignments, each of these alignments need not be tested separately.

The curved track geometry also applies to a number of these applications but in a more limited set of environments (e.g., rural setting versus freeway setting).

The intersecting geometry is unique in the sense that it must be tested in specific intersection situations.

3 Hardware Setup

The Federal Communications Commission (FCC) allows for a maximum equivalent isotropically radiated power (EIRP) transmission level of 33 dBm. The DENSO Wireless Safety Units (WSUs) used for these tests are capable of transmitting up to almost 20 dBm. In order to boost the signal strength to the maximum permissible value, the VSC-A team used a solid state power amplifier to generate a 33 dBm signal. The VSC-A team decided to use a General Dynamics Solid State Power Amplifier (Model LPCD6025R). Figure 1 depicts the transmitter setup, while Figure 2 shows the receiver.

These tests employed an antenna with 7 dB gain in the direction of maximum radiation and 0 dB gain in the horizontal direction. The antennas were mounted on the flat part of the roofs of the transmitting and receiving vehicles (see Figure 3), respectively, at the same height on each vehicle. Therefore, the horizontal plane transmission power is of primary interest. The transmission power reported for each test (e.g., 33 dBm) is the signal power into the antenna, which is equal to the power in the horizontal plane out of the antenna, and is, thus, 7 dB less than the EIRP.

The packet size in all tests was 400 bytes (including all overhead). For test efficiency, the sending WSU was configured to transmit as many packets per second as possible.

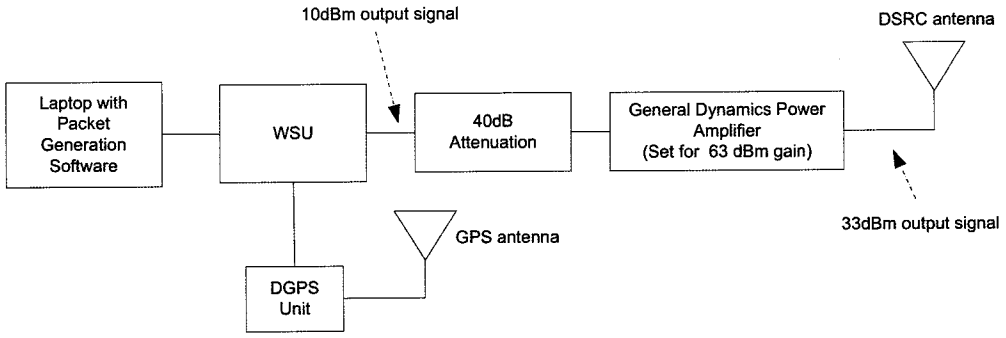

Figure 1: Transmitter Setup

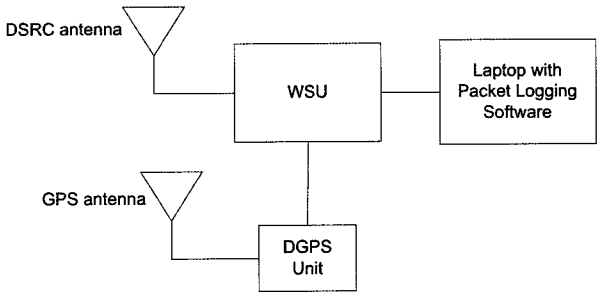

Figure 2: Receiver Setup

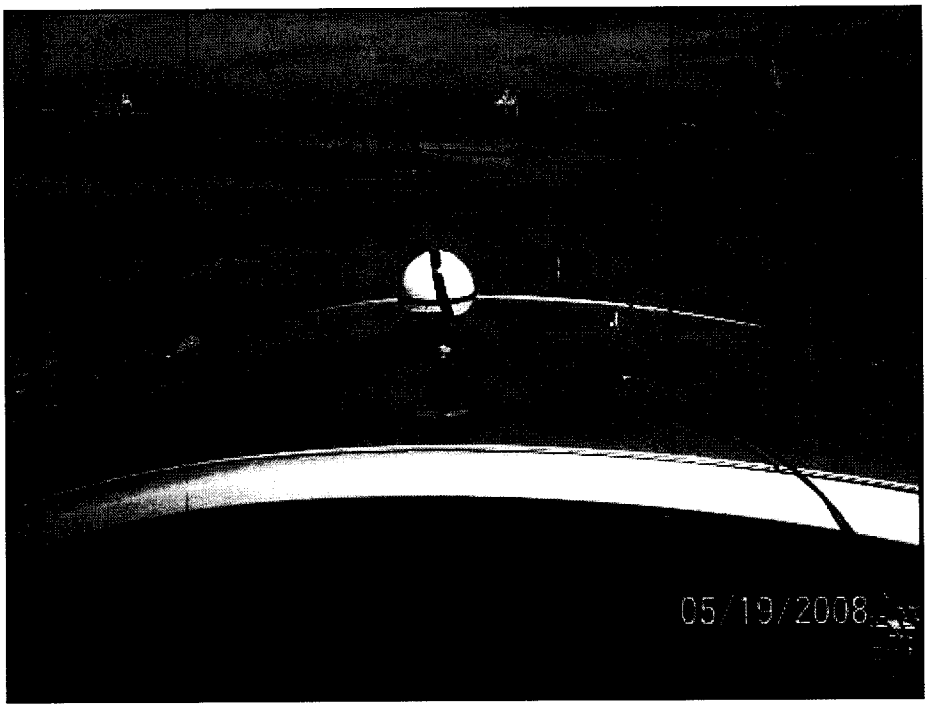

Figure 3: Transmit Vehicle Antenna Placement: DSRC (2, Black) and GPS (White Sphere)

3.1 Calibration

In order to validate the transmit power level, the setup was calibrated using a power meter. Figure 4 depicts how this was done. To ensure the validity of the results, the setup was recalibrated every time a new power level was chosen.

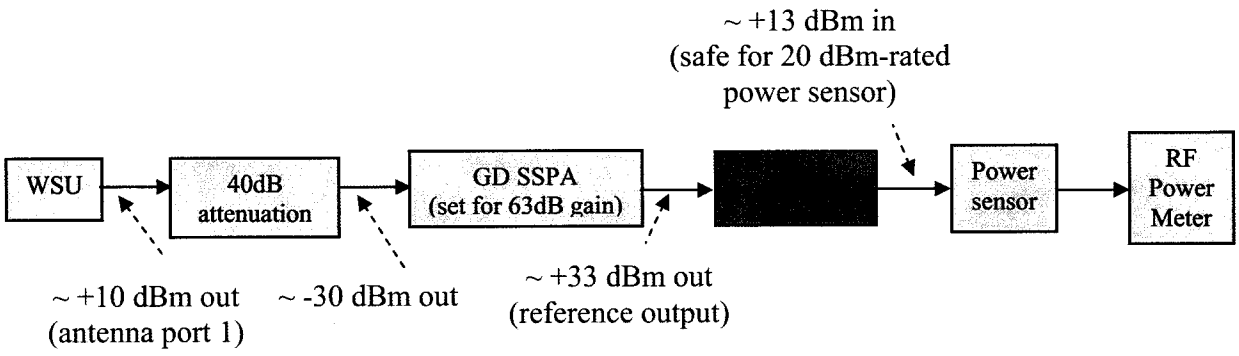

Figure 4: Calibration Using Power Meter

The use of a power amplifier on a signal induces nonlinearity. The Error Vector Magnitude (EVM) was measured in the transmitter setup both with and without the power amplifier. The setup and results are shown below in Figure 5 and Figure 6. Based on similar measurements reported to the VSC-A team by outside experts, EVMs in the range of 5-8 percent were expected. The team's EVM measurements, conducted both with and without the power amplifier attached to the WSU output, fell within that range.

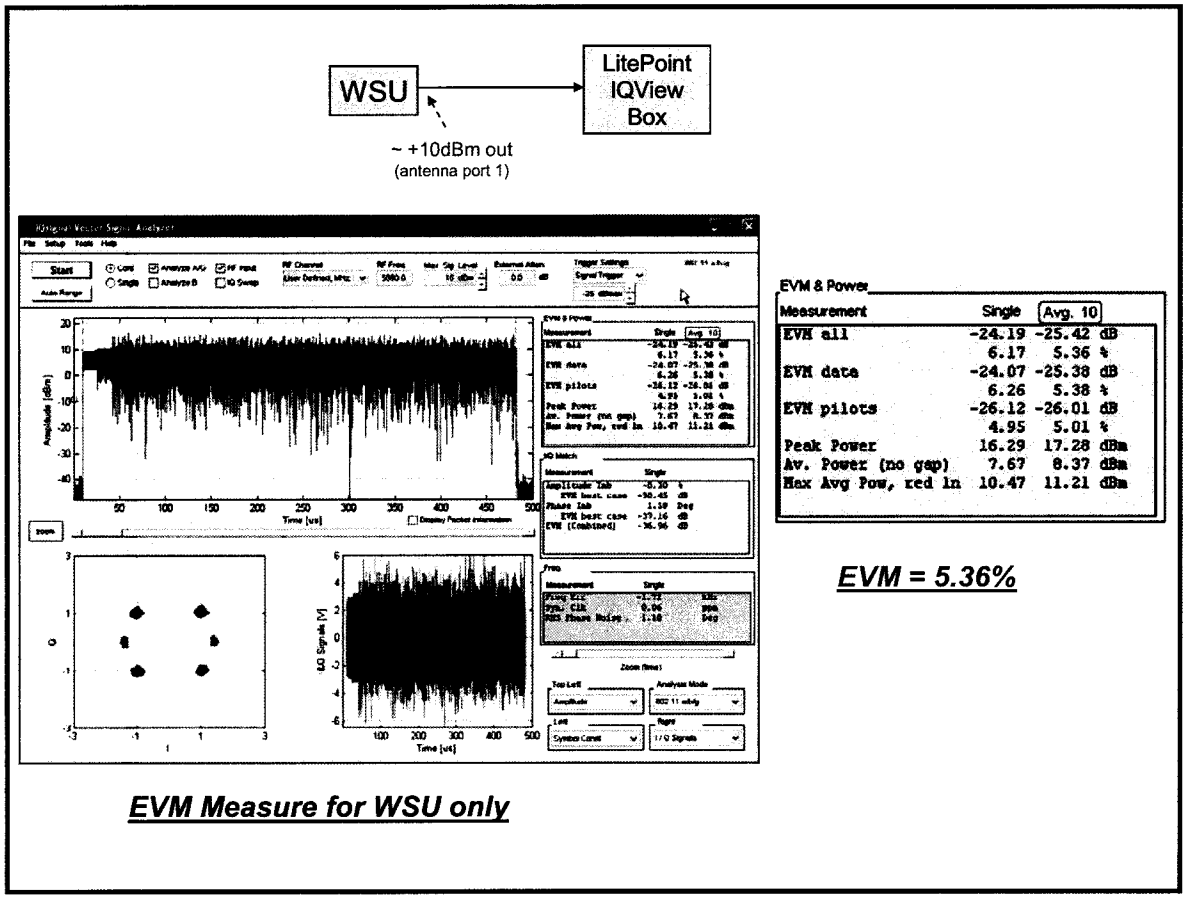

Figure 5: EVM Measure for WSU Only

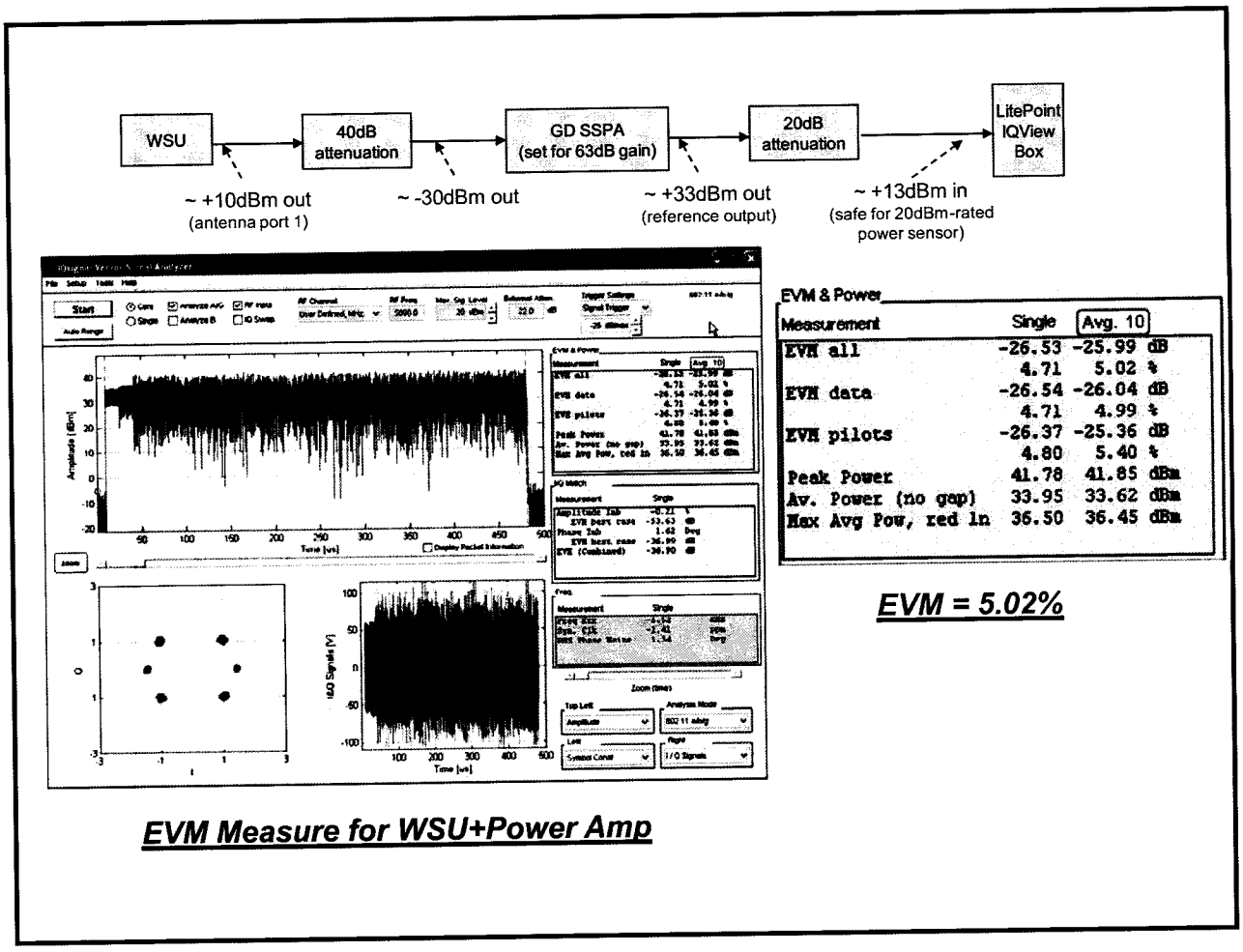

Figure 6: EVM Measure for WSU Connected to Power Amplifier

4 Test Results and Summary

The hardware setup was kept constant throughout the tests. Sixteen scenarios were tested. These are listed in Table 1. Each test scenario is reported in one of the sections 4.1-20 below. For each scenario the following details are presented:

1. Test location
2. Test settings and configuration
3. Description of any testing discrepancies
4. Graphical plots of the relationship between Packet Error Rate (PER) and distance, and Received Signal Strength Indication (RSSI) and distance
5. Observations that can be drawn from that test scenario

Table 1: Power Test Scenarios

Scenario
Baseline Line-of-Sight
Baseline Shadowing
Urban Straight Line
Urban Closed Intersection
Urban ¾ Open Intersection
Suburban Closed Intersection
Suburban ¾ Open Intersection
Rural Closed Intersection
Rural ¾ Open Intersection
Curved Road
Freeway Line of Sight
Rural Highway Line of Sight
Freeway Shadowing
Rural Highway Shadowing
Arterial Road Shadowing
Expressway Shadowing

4.1 Interpreting Data Graphs

PER is the primary performance metric used in this report. It is defined as the ratio of unsuccessful packet transmissions to total packet transmissions within a single test. A packet transmission is unsuccessful if the packet is either not received at all or is received with uncorrectable bit errors. PER plots tend to have high variance so it is hard to define a precise range of successful transmission. However, in each case PER tends to increase with increasing distance, and in most cases, there is a point beyond which communication is clearly unreliable.

The performance graphs in this report all use distance as the x-axis variable, either vehicle-to-vehicle distance or vehicle-to-intersection distance. In some cases a specific curve does not span the entire distance range of the x-axis. There are two reasons why this might be true for a given plot:

- Communication was not attempted for the particular configuration shown by the plot, but the distance was used in other tests reported in the same figure. An example of this can be seen in Figure 79. The PER curve labeled "ruralLOS-33dBm-6Mbps-1" stops between 300 m and 400 m, and the PER value never exceeds 4% below 300 m. In these cases it is not possible to say what the PER would be for distances greater than those included in the plot, except that PER generally grows with distance.
- The receive vehicle was unable to receive any packets from the transmit vehicle for distances beyond a certain threshold. An example of this can be seen in Figure 9. The PER curve labeled "var-LOS-5dBm-3Mbps-1" stops between 400 m and 600 m, after experiencing a rapid rise toward 100% between 200 m and

400 m. In these cases the PER should be considered 100% for distances greater than those included in the plot.

The tests reported in Sections 5-14 involve one stationary vehicle and one moving vehicle. In those tests, which are easy to repeat, the distance range tested is the same for all plots included in a given figure. So, in these sections a curve that stops before reaching the right edge of the graph could be explained only by the second reason above.

The tests reported in Sections 15-20 involve two vehicles moving in traffic. The varying distance between the vehicles was achieved by varying their relative speed (usually by varying the speed of the transmit vehicle), and tests were not easy to repeat. In particular, it was not always possible to exercise the same distance ranges for all tests plotted in a given figure. So, in these sections a curve that stops before reaching the right edge of the graph could be explained by either of the above reasons.

5 Baseline Line-of-Sight Scenario Tests

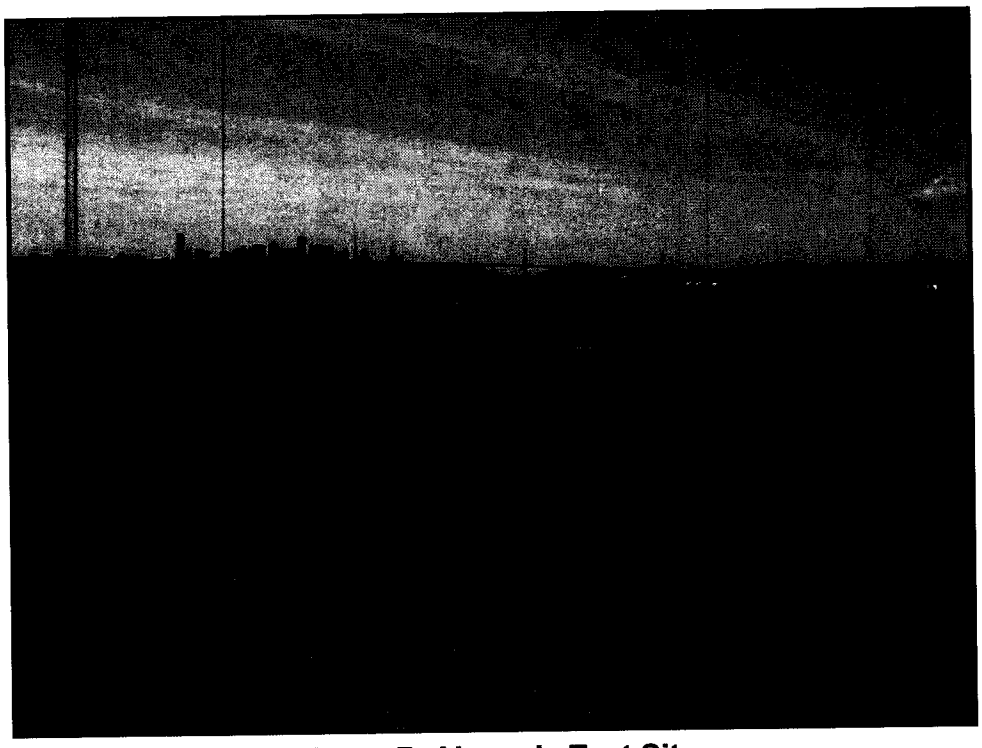

Figure 7: Alameda Test Site

Figure 7 shows the site for the baseline tests. The tests were conducted at an abandoned naval airstrip in Alameda, California. The runway was approximately 1 mile in length. The transmitter was kept stationary at the same location for all the tests. The receiver was initially placed at a distance beyond communication range. It moved toward the transmitter at a constant speed (10 mph or 20 mph)[1] for each of the test cases. Table 2

[1] In each test the WSU transmitter was configured to send approximately 1000 packets per second. At 10 mph relative vehicle speed, the inter-vehicle distance changes by about 5 meters per second.

below outlines the various test cases that were conducted for the Baseline Line-of-Sight (LOS) Scenario.

Table 2: Test Cases for the Baseline LOS Scenario

TX Power / Data Rate	5dBm	10dBm	15dBm	20dBm	26dBm	33dBm
3Mbps	Test 1	Test 4	Test 7	Test 10	Test 13	Test 16
6Mbps	Test 2	Test 5	Test 8	Test 11	Test 14	Test 17
12Mpbs	Test 3	Test 6	Test 9	Test 12	Test 15	Test 18

5.1 Location Overview

The airstrip served as a good location to conduct the baseline tests. There was clear LOS propagation between the transmitter and receiver from opposite ends of the air strip, and minimal sources of reflection. The team did note the presence of cargo ships in a channel adjacent to the airfield (see Figure 8) and recorded the movement of ships during the various tests. No correlation was found between ship presence and test outcomes. The nearest point between the channel and the transmit vehicle was about ½ mile. The nearest point between the channel and the receive vehicle was about ¼ mile, which occurred when the transmit and receive vehicles were at their maximum separation.

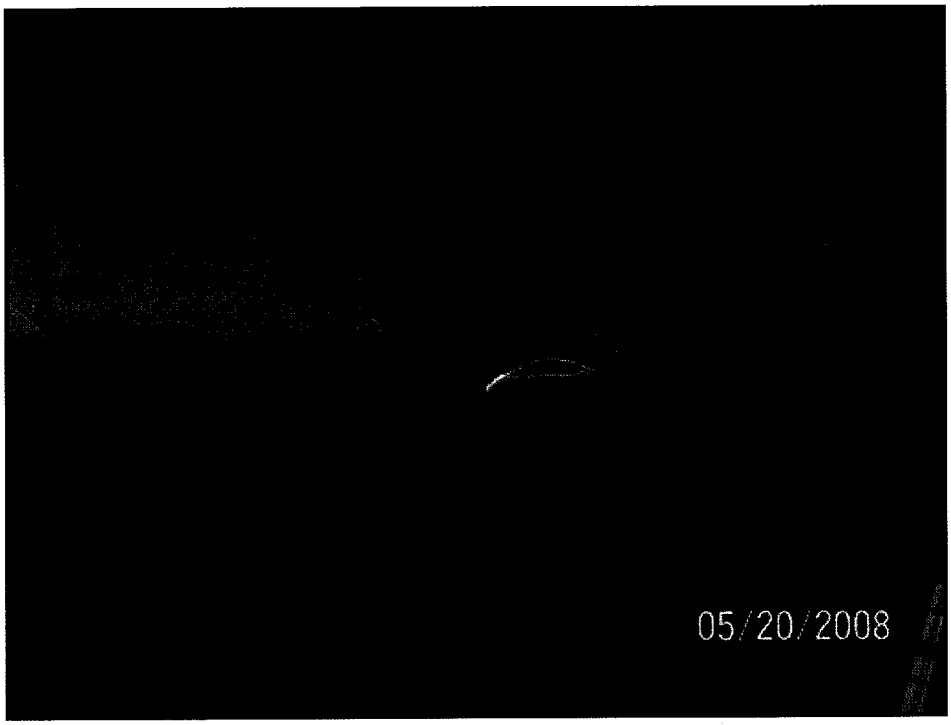

Figure 8: View of the Ships at the Test Site

5.2 Data Analysis

The results of the Baseline LOS tests conducted with a 3 Mbps bit rate are shown in Figure 9 and Figure 10. The first figure shows PER versus inter-vehicle distance for the

six transmit powers. At 33 dBm transmission power, communication becomes sporadic or worse beyond about 1300 meters. At 20 dBm, the packet error rate is high for distances greater than about 900 meters. At 5 dBm, PER is significant for distances greater than 200 meters.

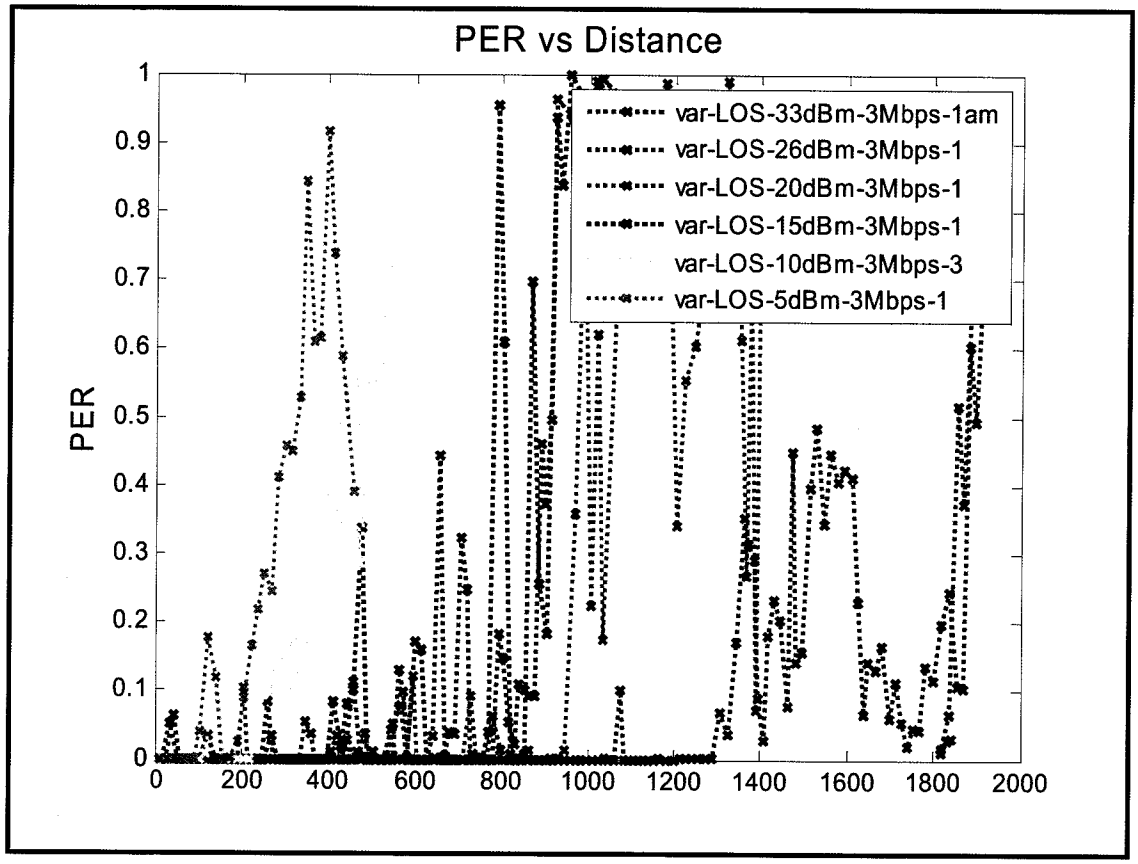

Figure 9: PER Versus Distance for Various Power Levels at 3 Mbps in Baseline-LOS Scenario

Figure 10 shows RSSI versus distance. In each case, the RSSI decays approximately exponentially with distance. Both plots show worse performance for 26 dBm than for 20 dBm. This anomaly was observed during testing and is discussed in Section 22.

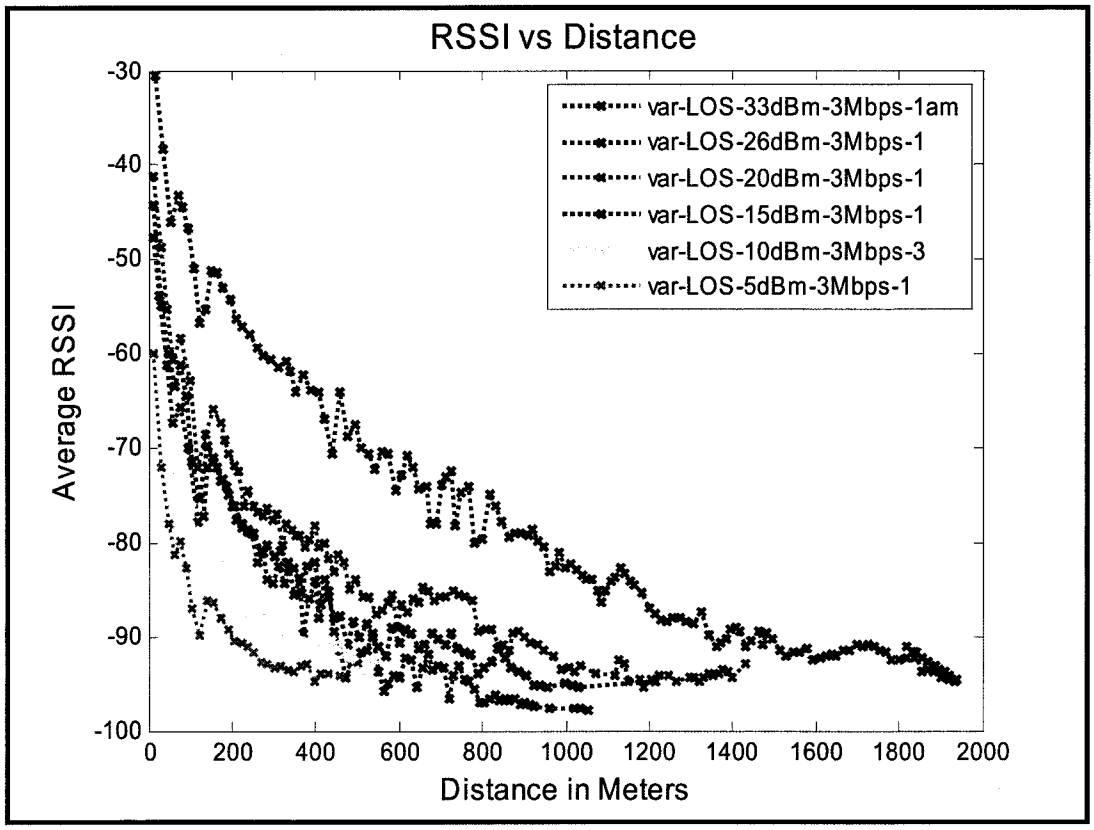

Figure 10: RSSI versus Distance for Various Power Levels at 3 Mbps in Baseline-LOS Scenario

5.3 Baseline LOS Scenario Observations

Figure 9 and Figure 10, along with other data collected in the Baseline LOS Scenario tests, lead to the following observations:

1. There is a clear dependence between power and range, with greater power leading to greater transmission range
2. Transmissions at higher data rates (6 Mbps and 12 Mbps) result in a drop in transmission range (6 Mbps and 12 Mbps baseline LOS results are not shown; similar results for 6 Mbps are shown in several sections below)
3. It is clear from Figure 9 that the PER curves exhibit high variability. This characteristic is inherent to the dynamic nature of the Radio Frequency (RF) propagation environment.
4. The PER curves make it difficult to identify a specific "reliable transmission range" for a given power. The range can be identified qualitatively as a region of rapid increase in PER, ignoring PER "bumps."
5. The RSSI curves are smoother and are representative of a 2-Ray Rayleigh fading environment. This is evident from the consistent dips in RSSI in the 100-200 meter range, which is a result of destructive interference at 5.9 GHz between the LOS wave and the wave reflected from the ground.

6 Baseline Shadowing Scenario Test

The Baseline Shadowing Scenario Tests were conducted at the same site as the Baseline LOS Scenario reported in the previous section (see Figure 7). In this test, the transmitter and receiver were initially placed at a distance out of communication range, and a semi-truck with 45 foot trailer was placed midway between the two vehicles. The transmitter was kept stationary at the same location for all the tests. The receiver moved toward the transmitter at a constant speed (20 mph) for each of the test cases, while the truck moved at roughly ½ the speed (10 mph). The 18 test cases shown in Table 2 were repeated for this scenario.

6.1 Data Analysis

Four graphs are shown in this section. The first two graphs (Figure 11 and Figure 12) show PER and RSSI, respectively, versus distance for various transmission powers. The second pair of graphs (Figure 13 and Figure 14) show PER and RSSI, respectively, for two powers and two bit rates (four total combinations).

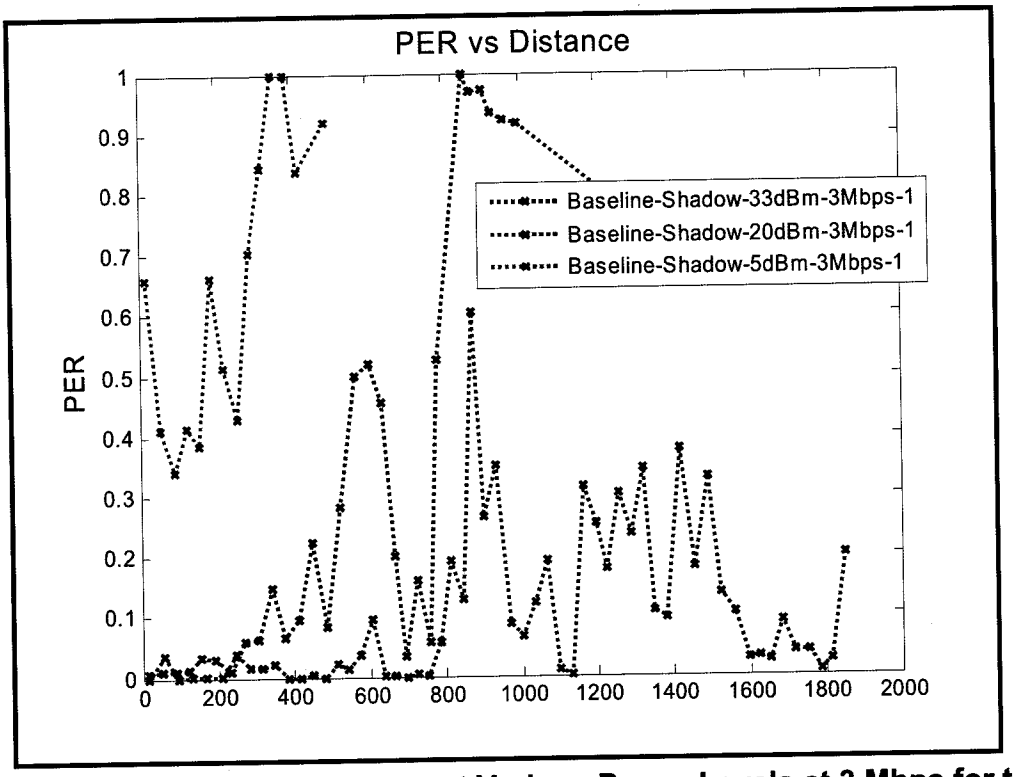

Figure 11: PER versus Distance at Various Power Levels at 3 Mbps for the Baseline-Truck Scenario

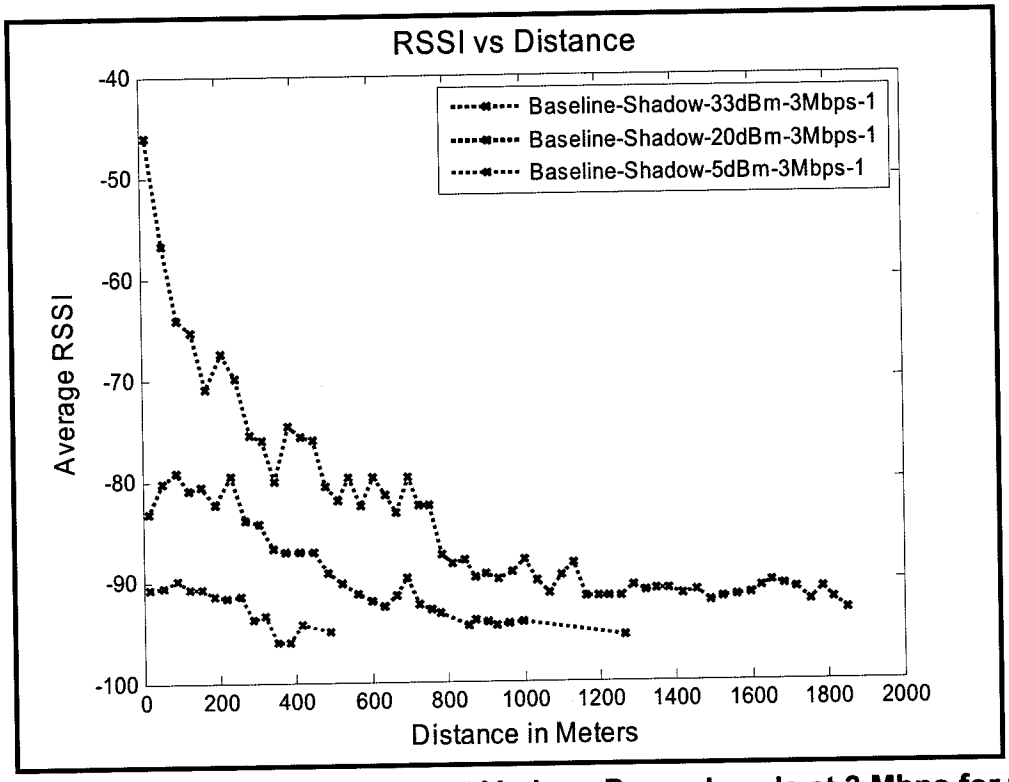

Figure 12: RSSI versus Distance at Various Power Levels at 3 Mbps for the Baseline-Truck Scenario

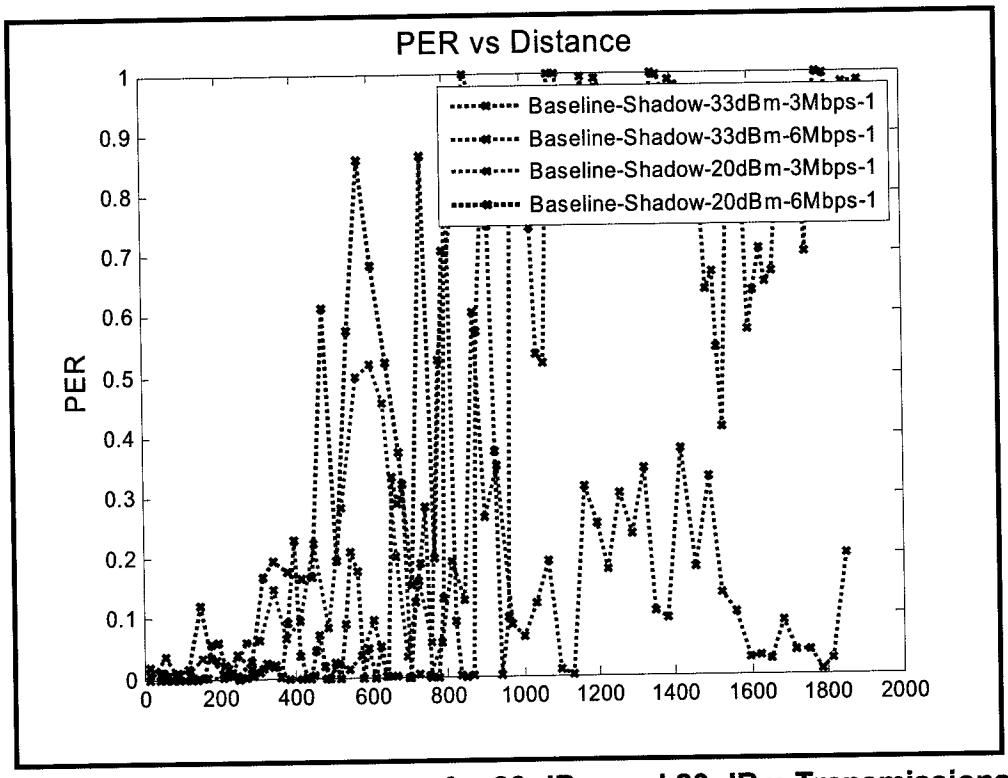

Figure 13: PER versus Distance for 33 dBm and 20 dBm Transmissions at 3 Mbps and 6 Mbps

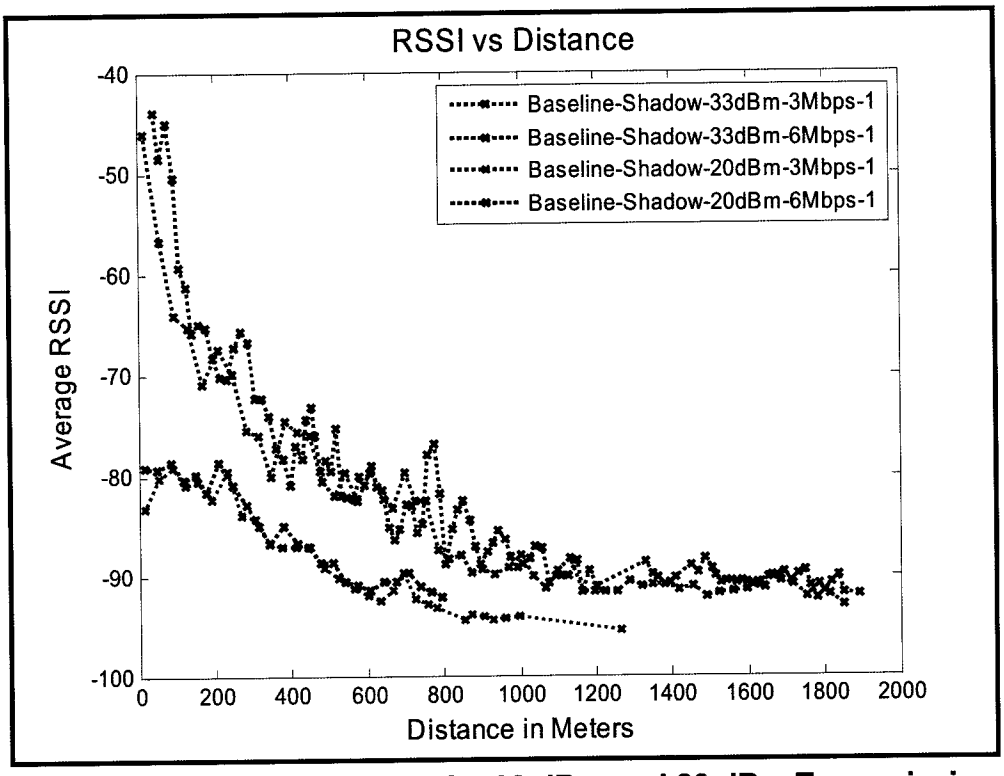

Figure 14: RSSI versus Distance for 33 dBm and 20 dBm Transmissions at 3 Mbps and 6 Mbps

6.2 Baseline Shadowing Scenario Observations

1. Figure 9 shows that at 20 dBm there is effective communication to approximately 900 meters. By comparison, as shown in Figure 11, testing scenarios with the truck indicate the 20 dBm transmissions experience significant PER levels from about 500 meters onward. Similarly, at 5 dBm, there is an effective range of approximately 200 meters without the truck and with the truck PER never falls below 30 percent.

2. The results with the presence of the truck are fairly consistent over the various transmission powers and data rates (i.e., higher power leads to longer range) and lower bit rate correlates with lower PER. In particular, the performance penalty for 6 Mbps versus 3 Mbps is relatively modest at 20 dBm, but is more significant at 33 dBm, as shown in Figure 13.

3. One interesting observation from these shadowing tests concerns performance as the receiver vehicle and truck reach the end of their approach to the transmitter vehicle. Note the increase in PER over the final 100 meters for the 5 dBm curve in Figure 11. Also note the RSSI reductions for both the 5 dBm and 20 dBm curves over that same range in Figure 12. In the 5 dBm case (and also the 10 dBm case, not shown), the RSSI decrease was enough to cause significant packet errors, while in the 20 dBm case, the Signal-to-Noise Ratio (SNR) was sufficient to keep PER low even with the reduced RSSI.

4. The strategy for the baseline shadowing test was to position the truck equidistant from the transmitter and receiver at all times. However, at large V2V distances, the truck contributed minimally as a Non-Line of Sight (NLOS) obstruction.

7 Urban-Straight-Line Scenario Test

The Urban-Straight-Line Scenario test was conducted in downtown San Jose, California, along Santa Clara Street. This scenario was motivated by the safety applications concerned with traffic traveling along a single axis. In this test case, both the transmitter and the receiver were initially parked next to each other. The transmitter drove down Santa Clara Street for about 600 meters and at which point the transmitter pulled over to the side of the street. The receiver then drove toward the transmitter to get an additional set of data points for the same test configuration. This procedure was repeated for the test cases shown in Table 3.

Table 3: Test Cases for the Urban-Straight-Line Scenario Test

TX Power / Data Rate	10dBm	20dBm	33dBm
3Mbps	Test 1	Test 3	Test 5
6Mbps	Test 2	Test 4	Test 6

7.1 Location Overview

Santa Clara Street in San Jose is fairly representative of a typical downtown scenario with a moderate-to-high level of traffic and reasonably tall buildings along both sides. Figure 15 and Figure 16 show the propagation environment along the test area. The stretch of Santa Clara Street that could be categorized as an urban setting was about 600 meters long. For this reason, the communication ranges were not measured beyond 600 meters.

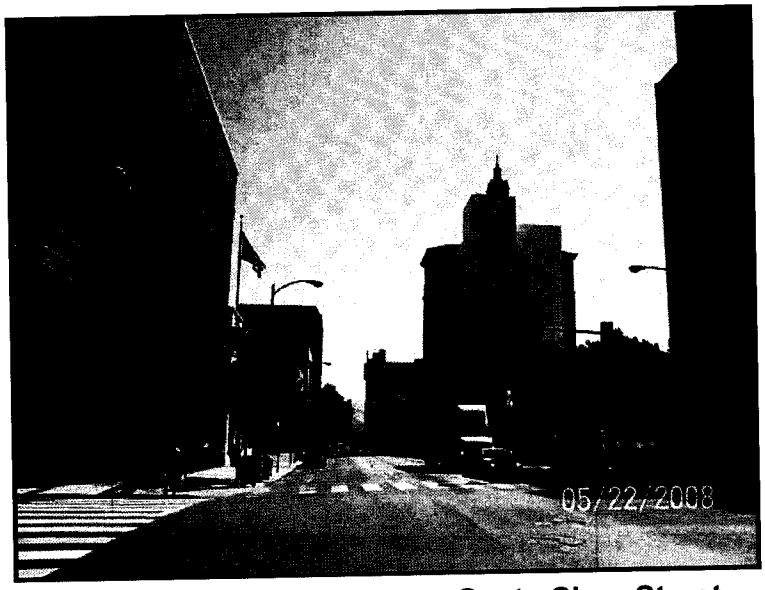

Figure 15: Looking East on Santa Clara Street

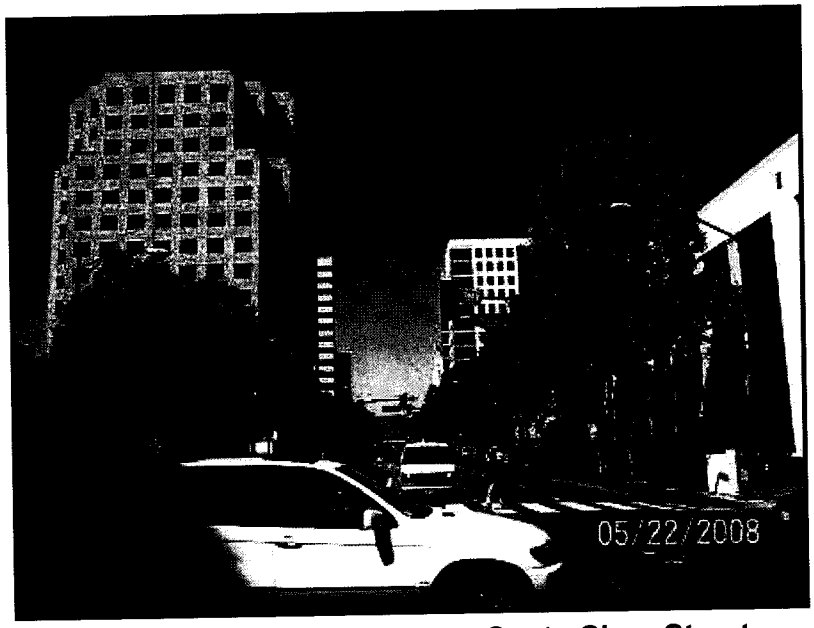

Figure 16: Looking West on Santa Clara Street

7.2 Data Analysis

Figure 17 and Figure 18 show the PER versus distance and RSSI versus distance curves for the straight-line urban tests. Figure 19 and Figure 20 compare operation at 3 Mbps and 6 Mbps, using 33 dBm and 20 dBm powers as test cases.

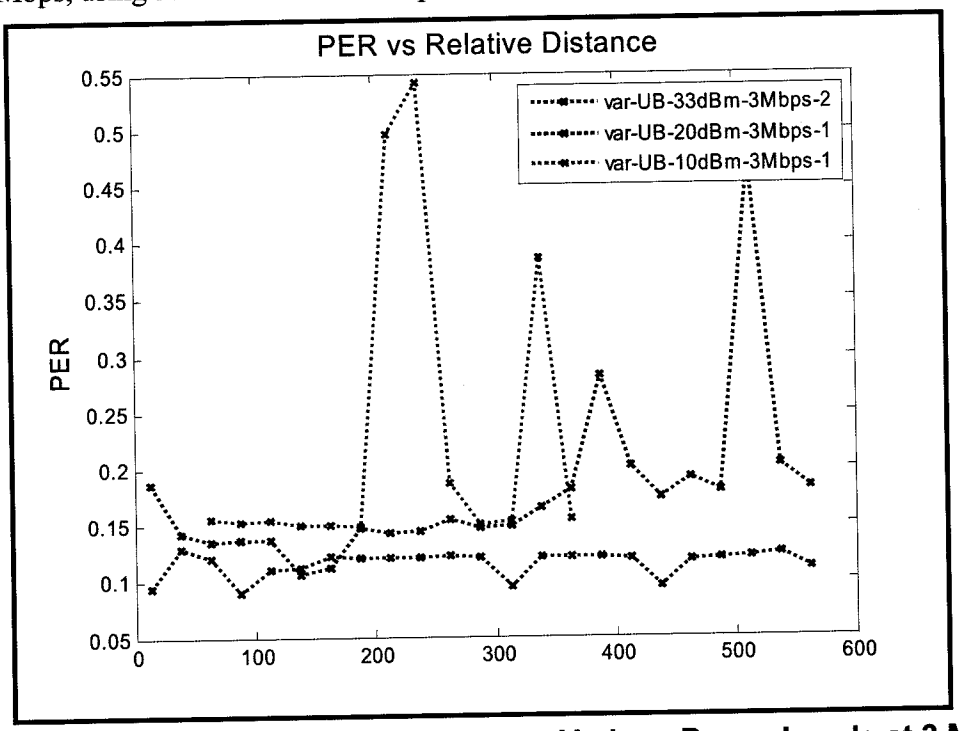

Figure 17: PER versus Distance Curves at Various Power Levels at 3 Mbps for the Urban-Straight-Line Scenario

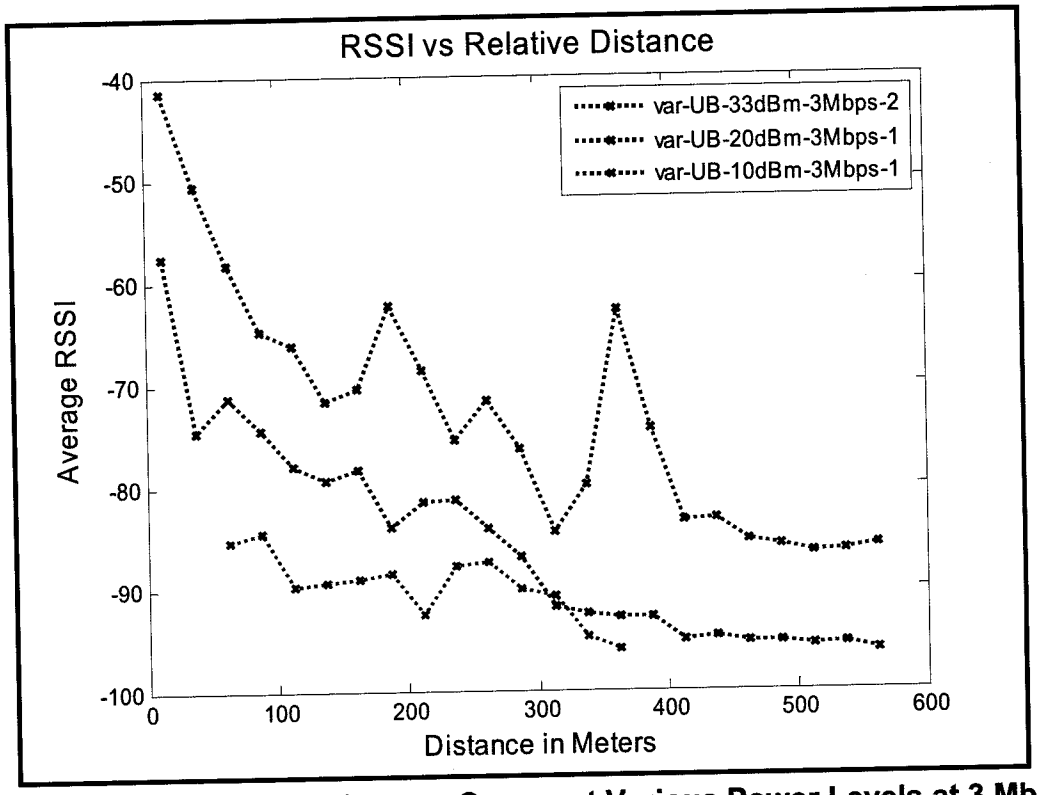

Figure 18: RSSI versus Distance Curves at Various Power Levels at 3 Mbps for the Urban-Straight-Line Scenario

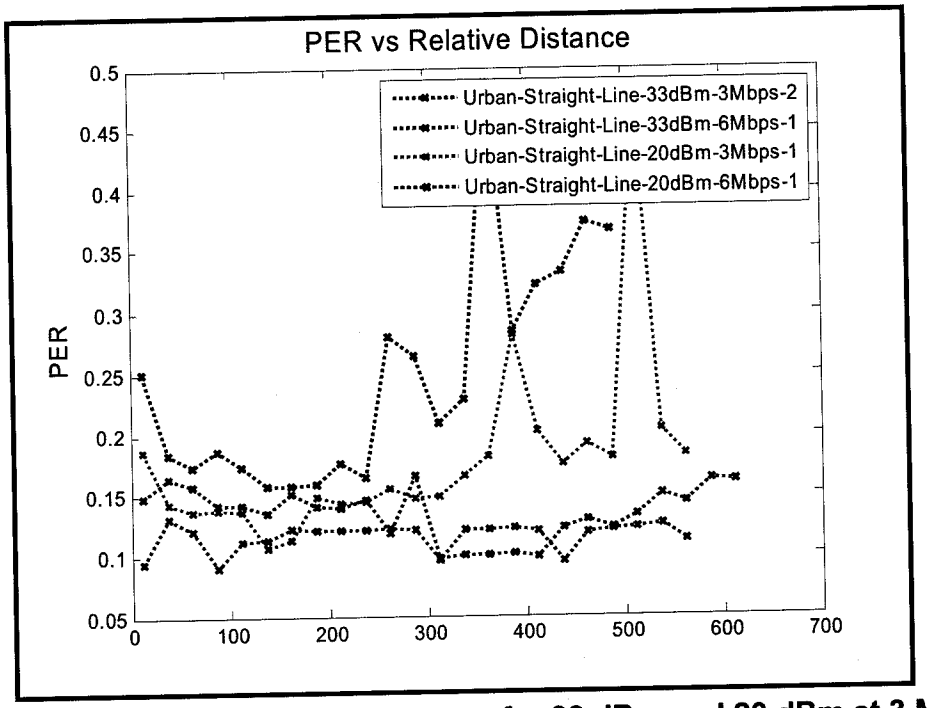

Figure 19: Comparison of PER Curves for 33 dBm and 20 dBm at 3 Mbps and 6 Mbps

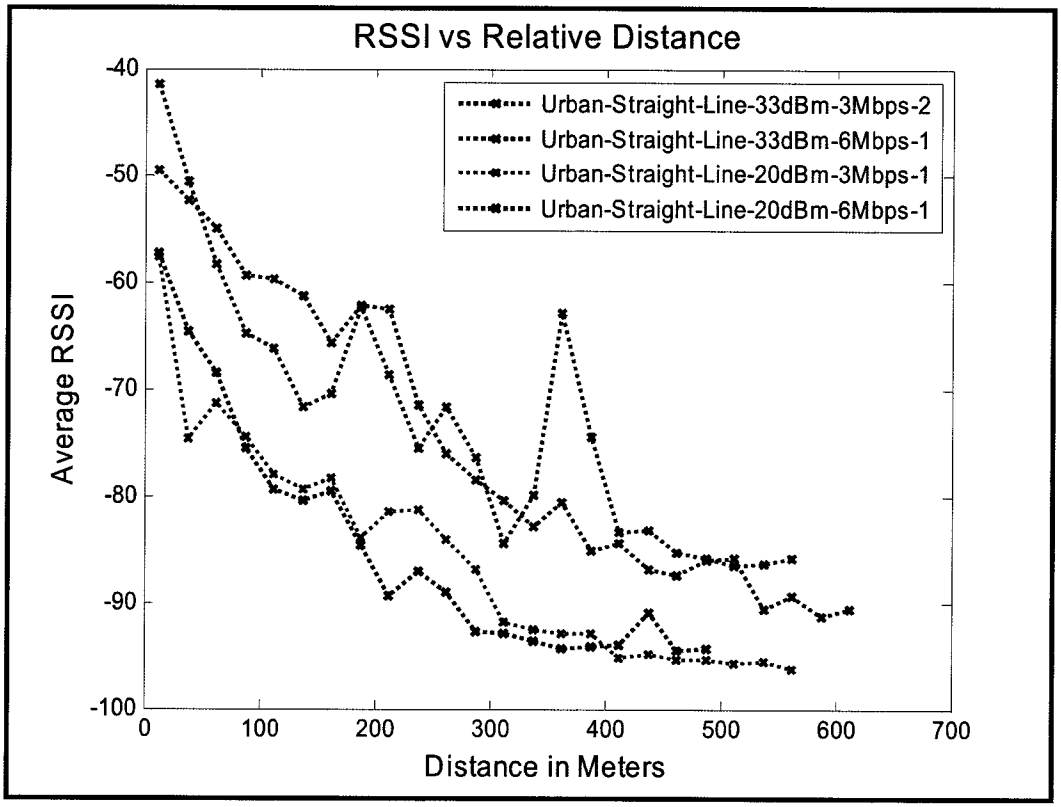

Figure 20: Comparison of RSSI Curves for 33 dBm and 20 dBm at 3 Mbps and 6 Mbps

7.3 Urban-Straight-Line Scenario Observations

1. At 33 dBm and 3 Mbps there is a fairly consistent PER between 10 percent and 15 percent across the entire 0-600 meter range. The non-trivial minimum PER contrasts with the two baseline scenarios, both of which saw PER approach zero as the inter-vehicle distance went to zero. In this case, the persistent 10 percent PER floor might be attributable to multipath due to building and vehicle reflections in the urban environment. The lower transmit powers exhibited a non-zero PER floor as well, and in the 10 dBm case, it was a bit higher, on the order of 15 percent.
2. The 10 dBm power level had a range of about 200 meters. For 20 dBm, communication became unreliable between about 400 and 500 meters. It is unclear whether the longer range associated with 33 dBm is warranted for the applications that would be active in this environment.
3. 6 Mbps transmissions performed somewhat worse than 3 Mbps transmissions at both 33 dBm and 20 dBm, but not dramatically so.

8 Urban-Closed-Intersection Scenario Test

The Urban-Closed-Intersection Scenario test was conducted in downtown San Jose, California, on the corner of Market Street and Santa Clara. This and the other intersection scenarios below were motivated specifically by intersecting geometry safety application(s). This test is categorized as a *closed*-intersection test because of the presence of (reasonably) tall buildings on all four corners of the Market-Santa Clara intersection. The transmitter-to-intersection distance was set at 5 fixed points (0 meters, 25 meters, 50 meters, 100 meters, and 150 meters), while the receiver drove toward the intersection on Santa Clara Street at the speed of traffic in each test. The test cases outlined in Table 4 were repeated three times for each of the transmitter positions.

Table 4: Test Cases for the Urban-Closed–Intersection-Scenario

TX Power / Data Rate	10dBm	20dBm	33dBm
3Mbps	Test 1	Test 3	Test 5
6Mbps	Test 2	Test 4	Test 6

8.1 Location Overview

Figure 21 shows the propagation environment along Market Street. The transmitter was parked at fixed locations along this street. The buildings on the right-hand side of the street served as obstructions between the transmitter and receiver (moving down Santa Clara Street). The photo shows the farthest of the five fixed positions, 150 meters from the intersection.

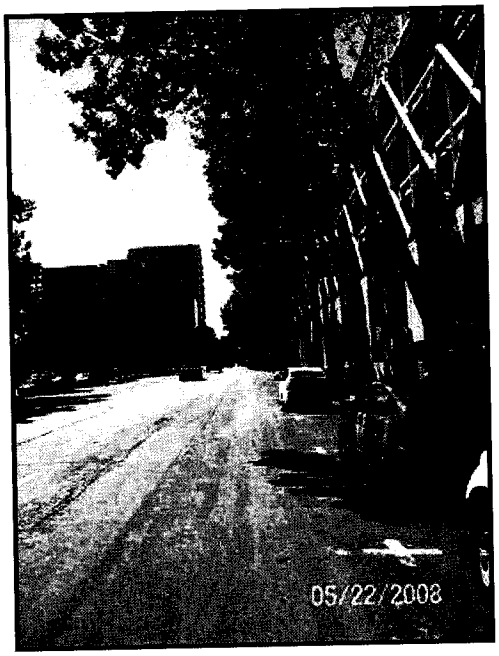

Figure 21: Looking South on Market Street toward the Intersection from 150 Meters

The buildings on the corner of the Market Street and Santa Clara Street intersection served as the primary obstruction between the two vehicles. The receiver approached the intersection heading east along West Santa Clara Street.

8.2 Data Analysis

Figure 22 and Figure 23 show PER and RSSI versus receiver-to-intersection distance curves for a 33 dBm transmission at various transmitter locations (indicated in the legend). Communication performance becomes worse as the transmitter moves away from the intersection.

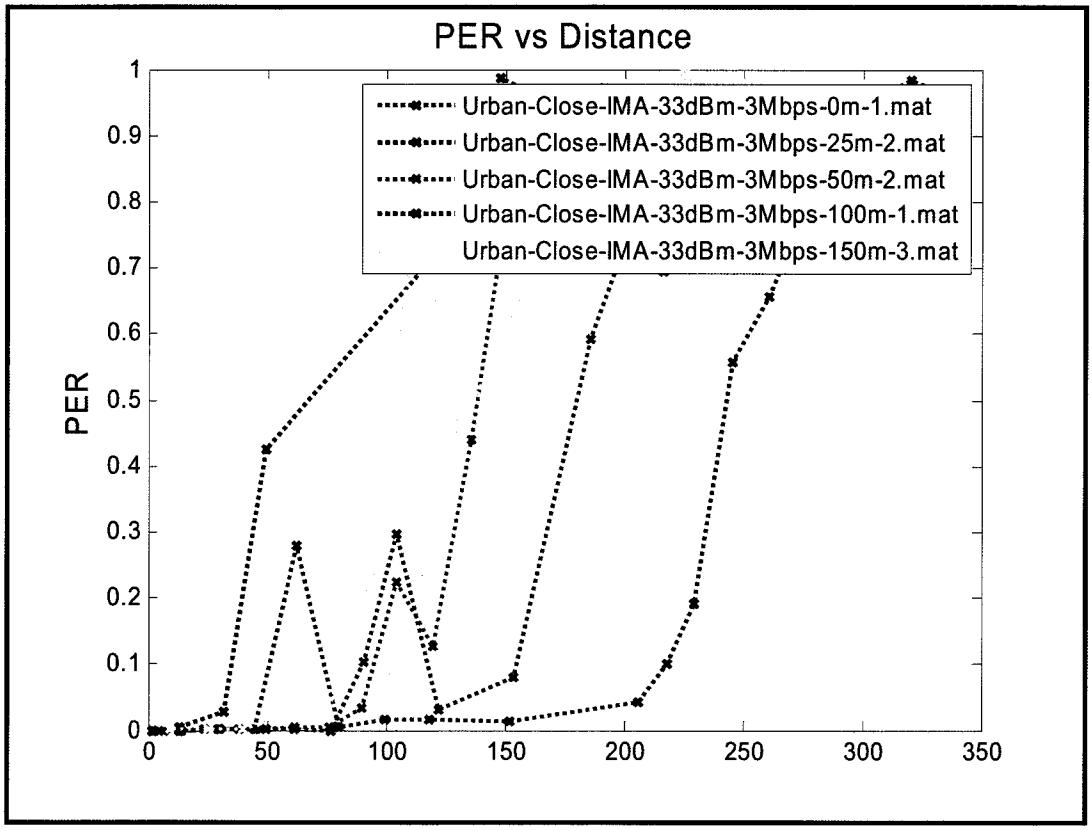

Figure 22: PER versus Distance Curve at 33 dBm and 3 Mbps for all the Different Transmitter Positions

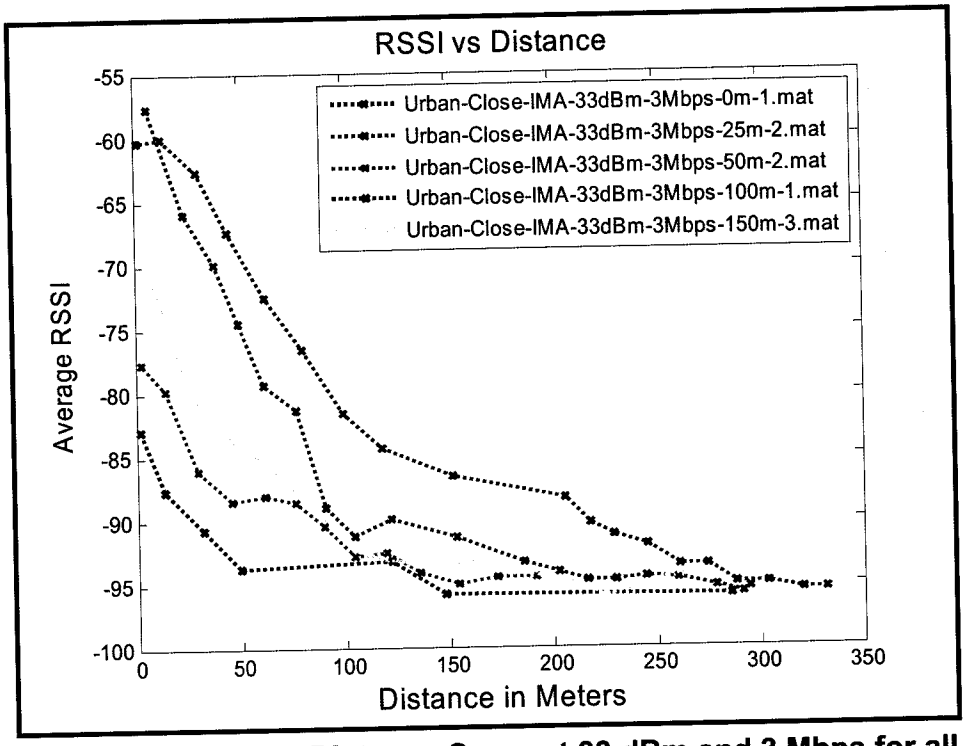

Figure 23: RSSI versus Distance Curve at 33 dBm and 3 Mbps for all the Different Transmitter Positions

Similar trends can be observed for 20 dBm transmissions (Figure 24 and Figure 25). It is clear that 33 dBm transmissions lead to increased reliability in intersection scenarios. The increased reliability of 33 dBm transmissions can be seen directly in Figure 26 and Figure 27, which compare communication performance at 10 dBm, 20 dBm, and 33 dBm.

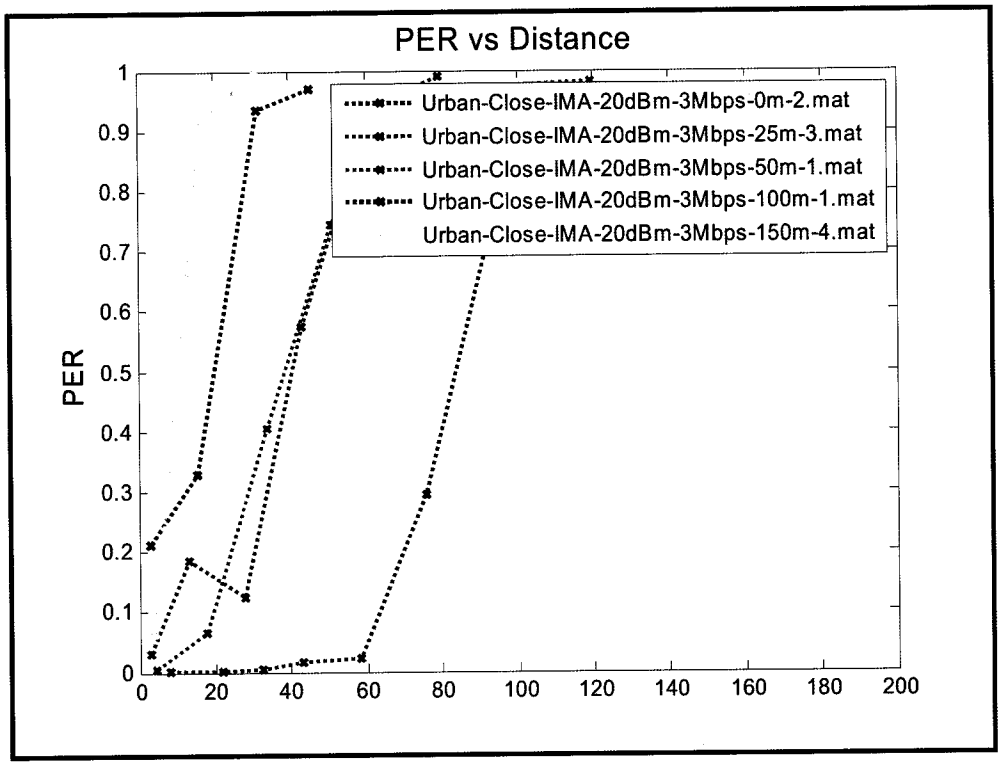

Figure 24: PER versus Distance Curve at 20 dBm and 3 Mbps for all the Different Transmitter Positions

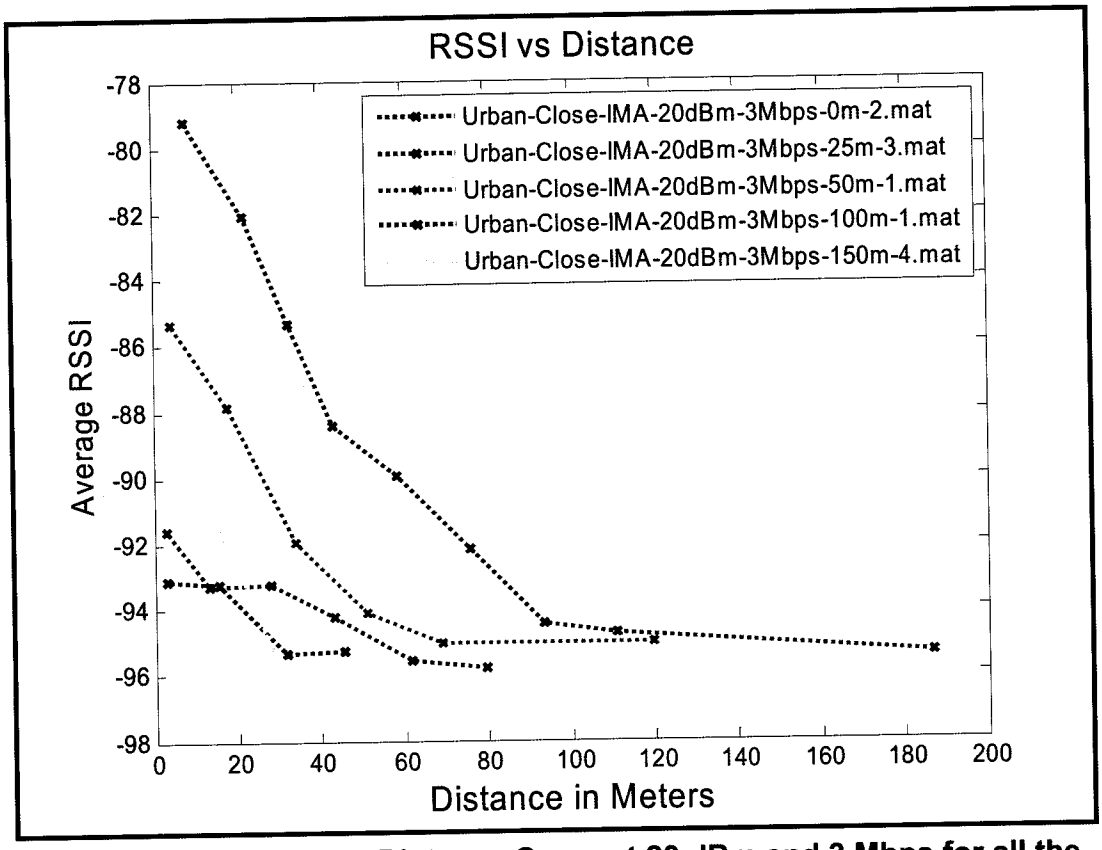

Figure 25: RSSI versus Distance Curve at 20 dBm and 3 Mbps for all the Different Transmitter Positions